SPHERE/ZIMPOL

H.M. Schmid, Institute for Particle Physics and Astrophysics, ETHZ

SPHERE VLT "Planet Finder":

overview

SPHERE/ZIMPOL technical performance

some ZIMPOL commissioning and early science results

ZIMPOL PSF characteristics

SPHERE visual coronagraph

ZIMPOL polarimetry

Search for planets in reflected light

Scattered light from circumstellar disks

SPHERE “VLT planet finder”

- 2^{nd} generation VLT instrument
- call for proposals around 2002
- first light in 2014

} long history

SPHERE = Spectro-Polarimetric High-contrast Exoplanet REsearch

Consortiuum:

Grenoble, Marseille, Paris, Nice (F), Heidelberg (D), Padova (I),

Geneva, Zurich (CH), NOVA-ASTRON, Amsterdam (NL)

- many people involved

SPHERE “VLT Planet Finder”

Extreme adaptive optics system for hight contrast imaging of extra-solar planetary systems

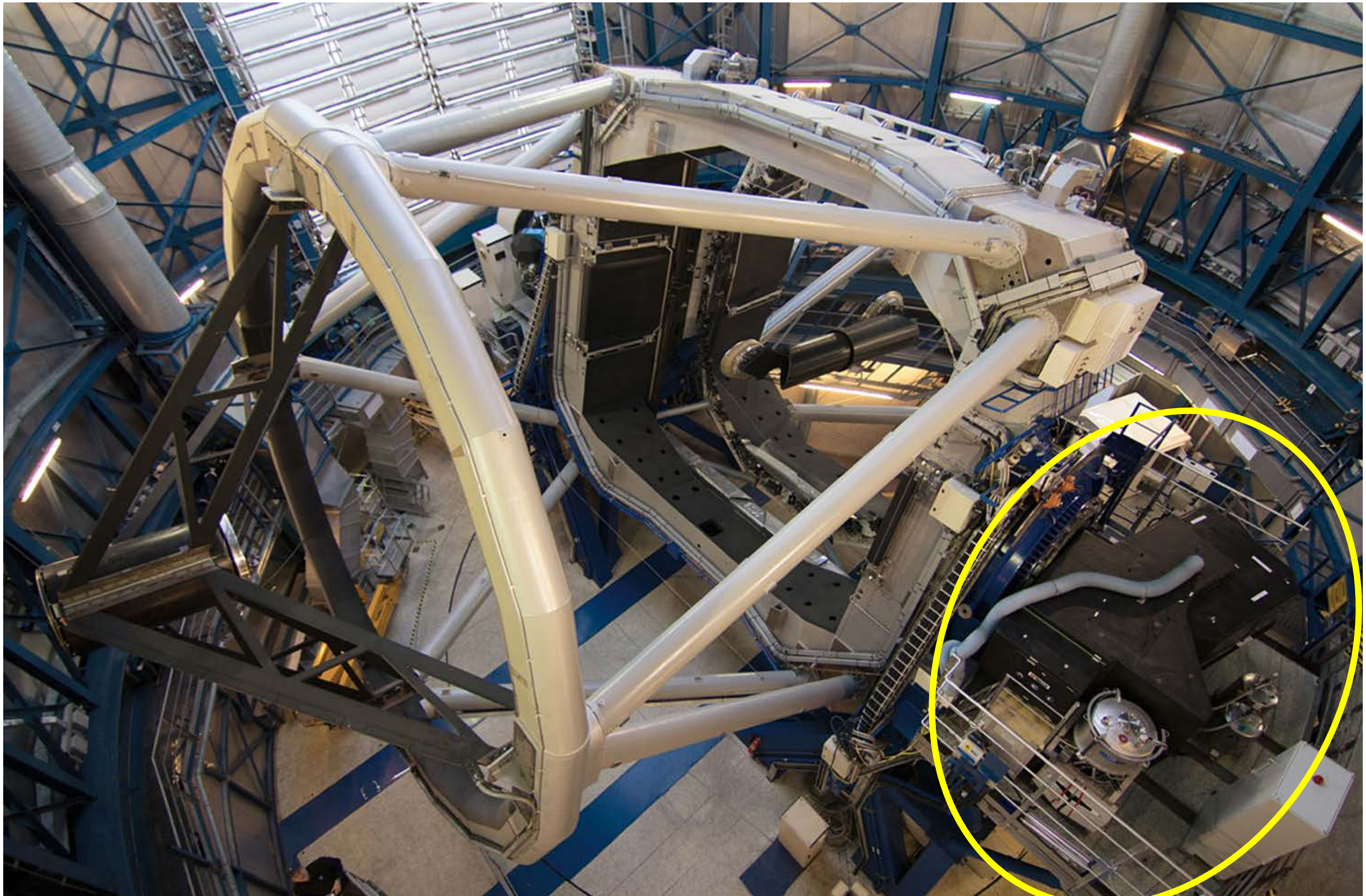

First extra-solar planet discovered by the SPHERE "Planet Finder"

Chauvin and 122 Co-Authors (2017)

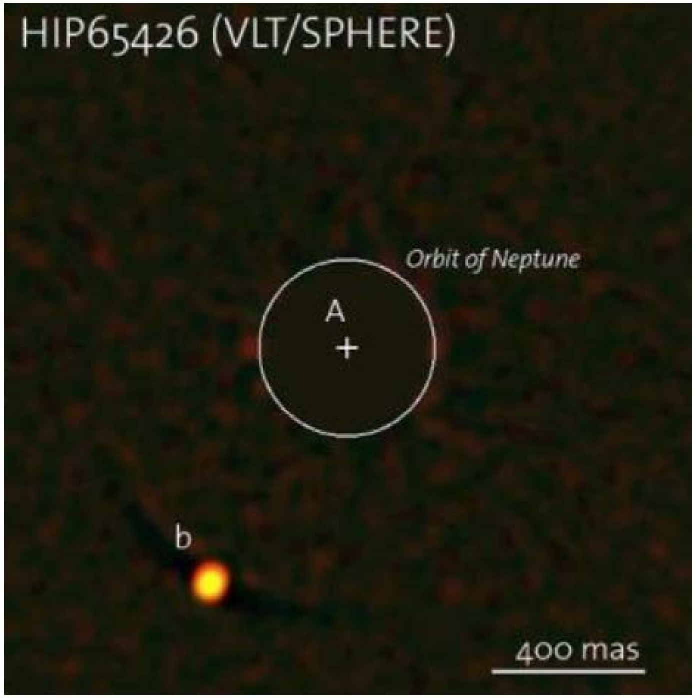

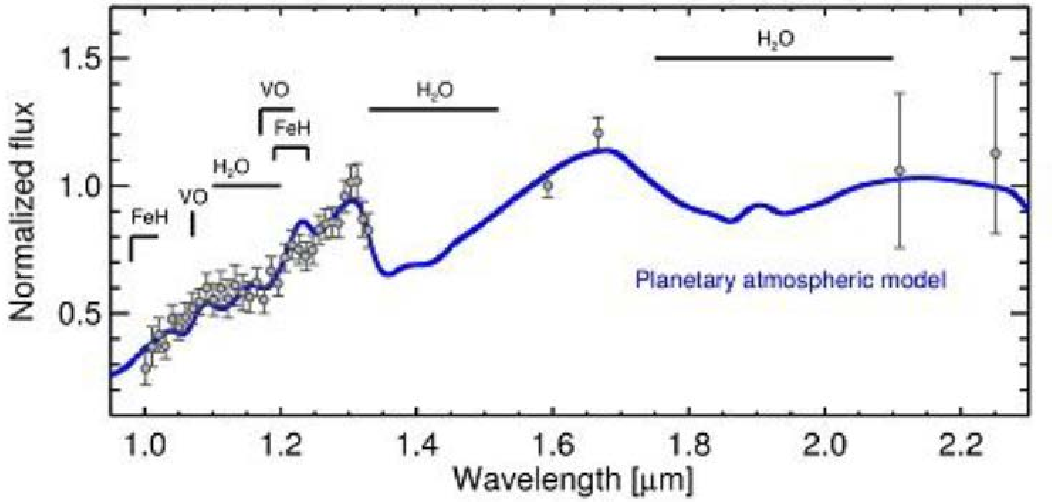

Caption: Light spectrum of exoplanet HIP65426b in the near-infrared region showing the presence of water i
spectrum can be seen as the 'fingerprint' of the exoplanet.
© ESO/SPHERE Consortium/G. Chauvin et al.

Planet: L6-dwarf, 6-12M_J, 1500 K, 17 Myr old, at 90AU around A2 star, at 110pc, young Sco-Oph association

Example: sun – jupiter system (5 pc)
star – young “jupiter” (50pc)

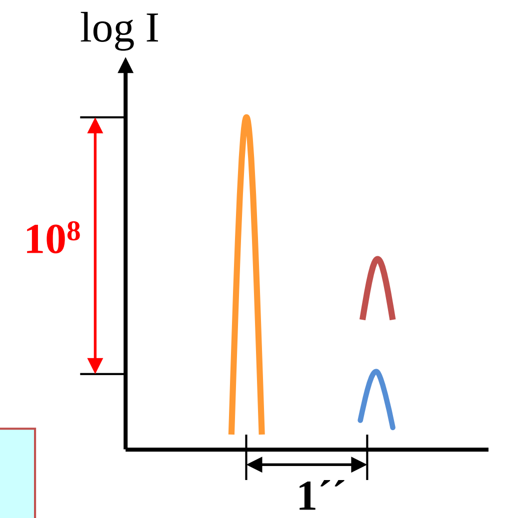

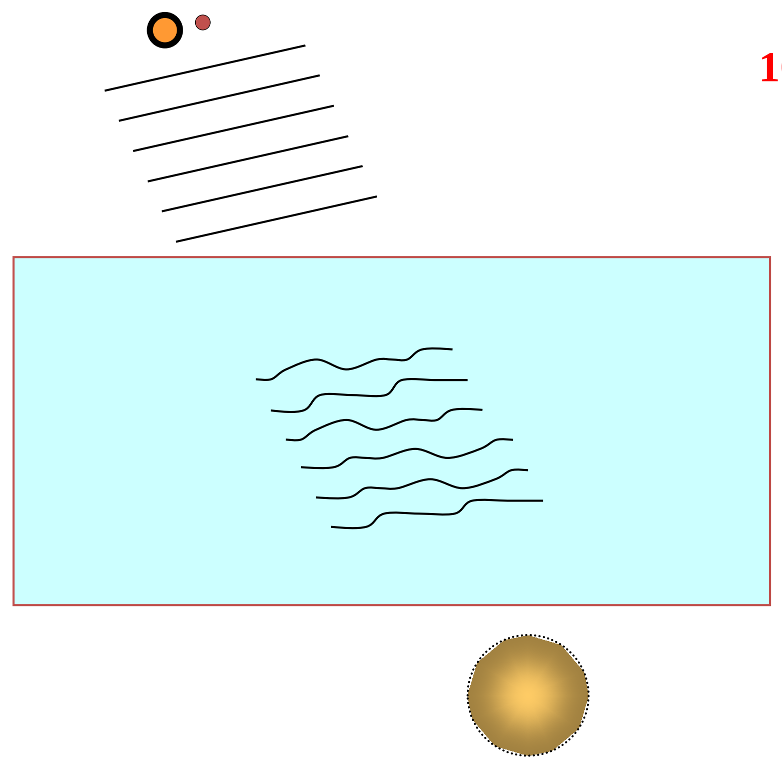

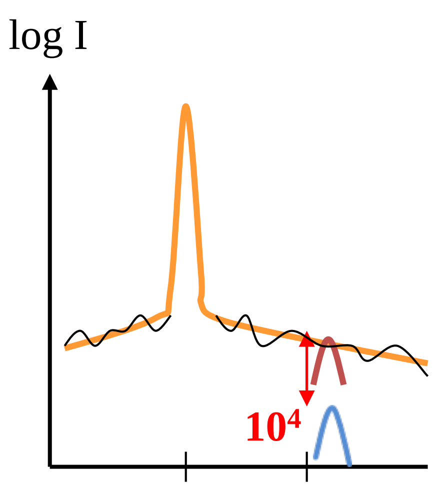

X-AO

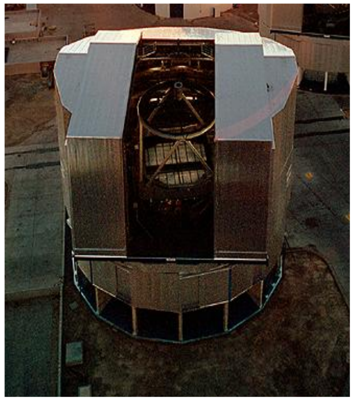

weak planet signal in variable
(residual) halo of the star

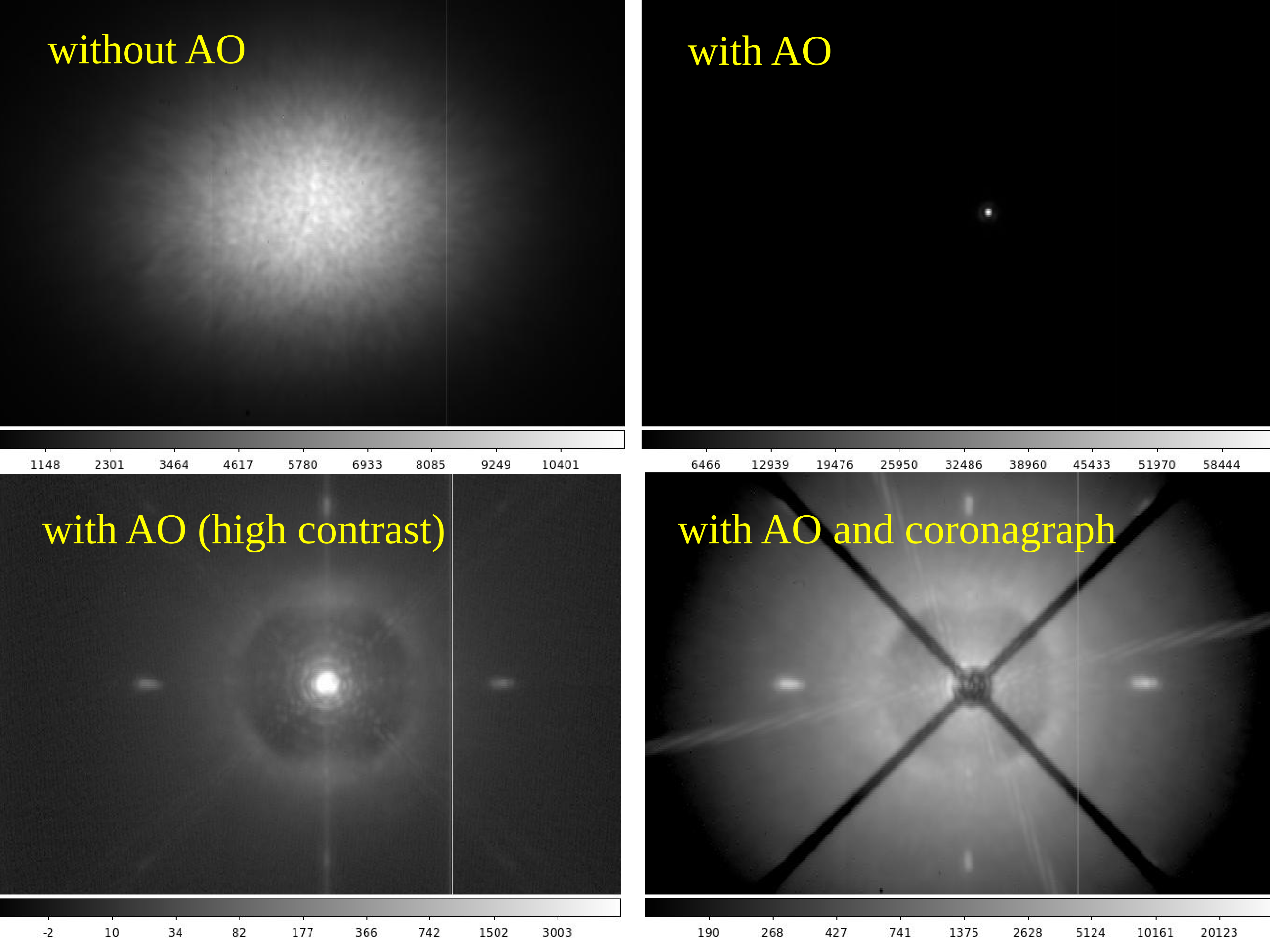

without AO
1148 2301 3464 4617 5780 6933 8085 9249 10401
with AO
6466 12939 19476 25950 32486 38960 45433 51970 58444
with AO (high contrast)
-2 10 34 82 177 366 742 1502 3003
with AO and coronagraph
190 268 427 741 1375 2628 5124 10161 20123

SPHERE block diagram

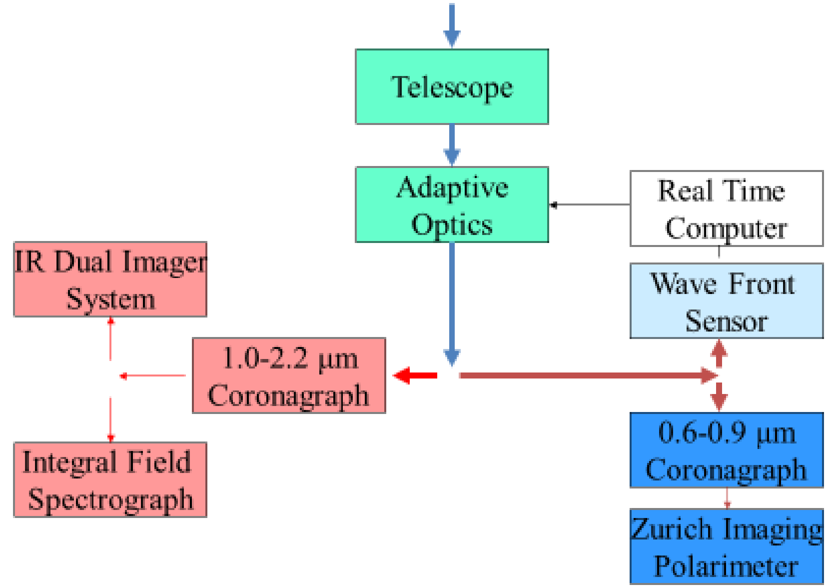

IMPLEMENTATION

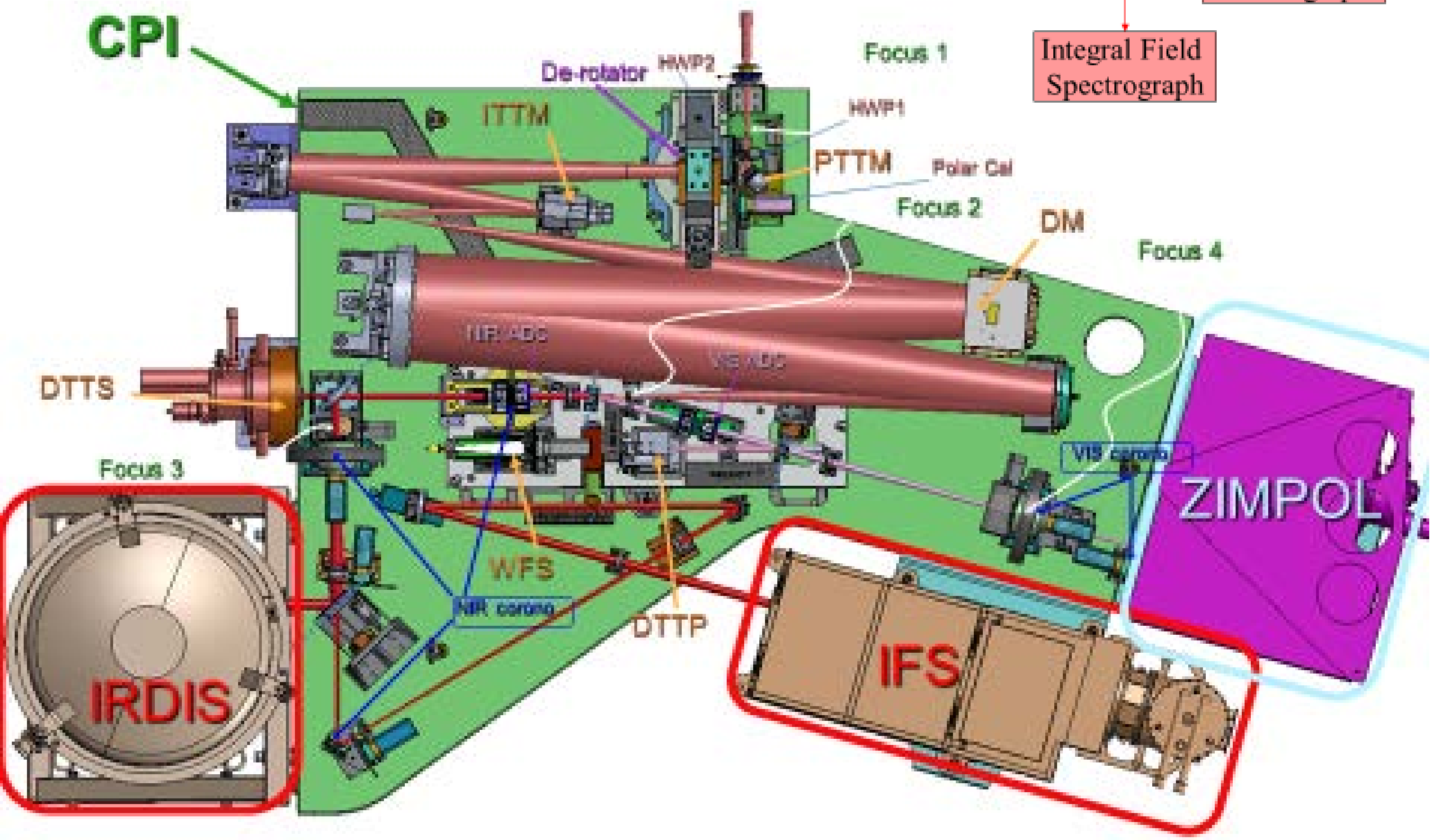

ZIMPOL as high resolution imager for λλ 500-900 nm

de Zeeuw, 2016, ESO messenger

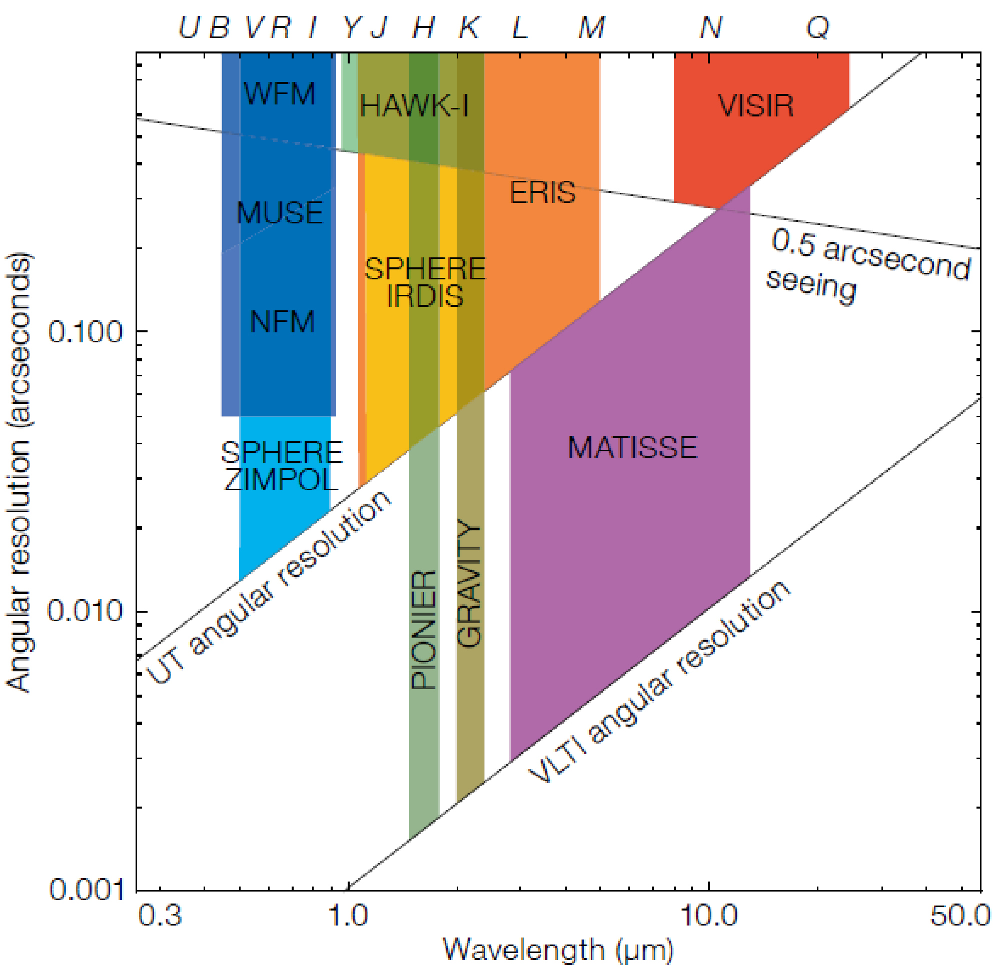

Figure 4. The angular resolution versus wavelength plane of the current and planned VLT and VLTI imaging instruments.

resolution ≈ λ/D

→ 20-30 milli-arcsec

→ V-band

→ Hα, ([O I], Na/HeI)

Commissioning and early science results

Spatial resolution: Comparison with HST

Symbiotic Mira variable R Aqr

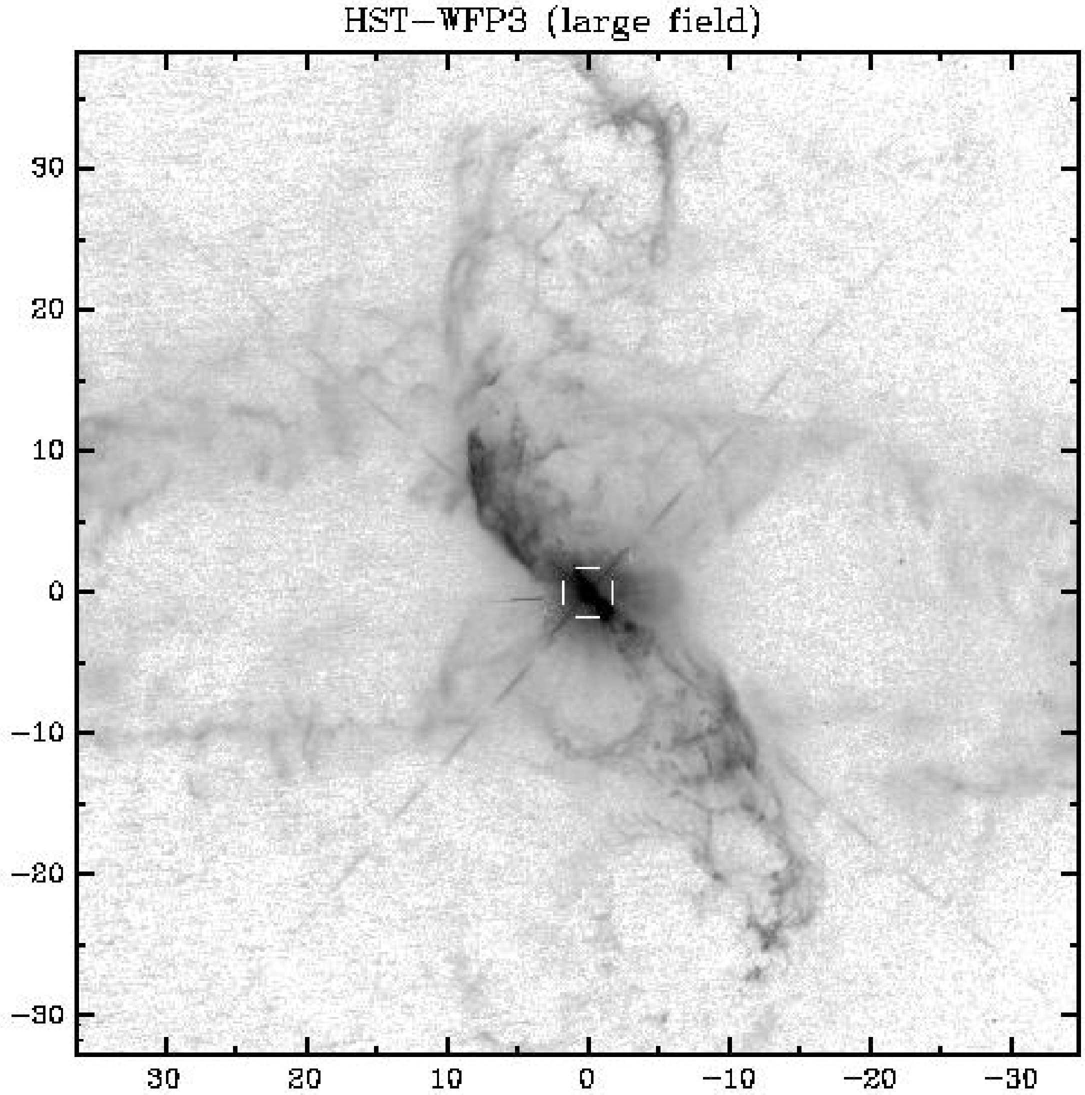

High Resolution: Hα for R Aqr (binary with jet)

HST: 80 milli-arcsec

SPHERE/ZIMPOL: 25 milli-arcsec

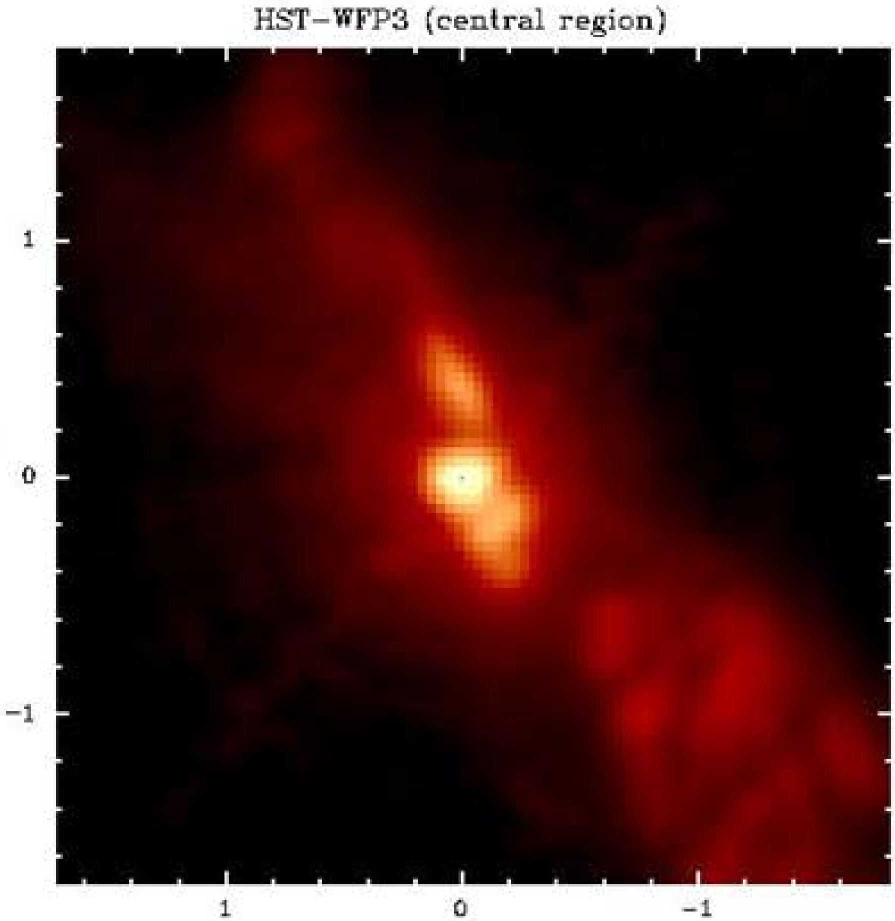

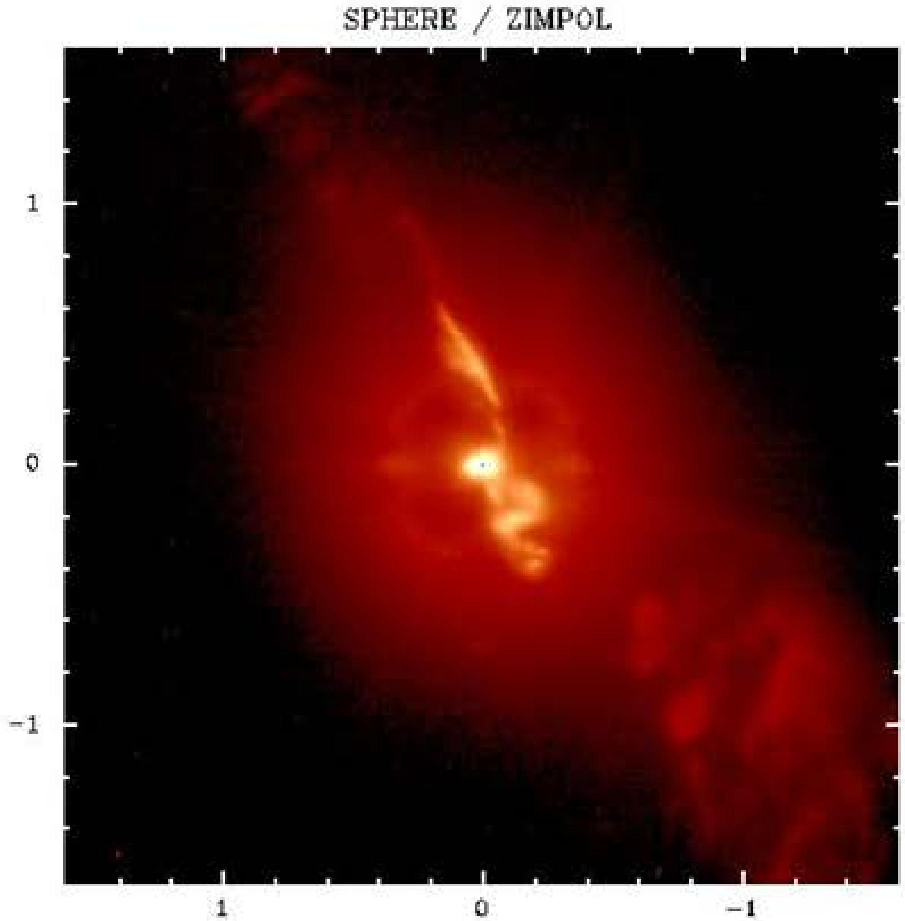

Schmid et al., 2017

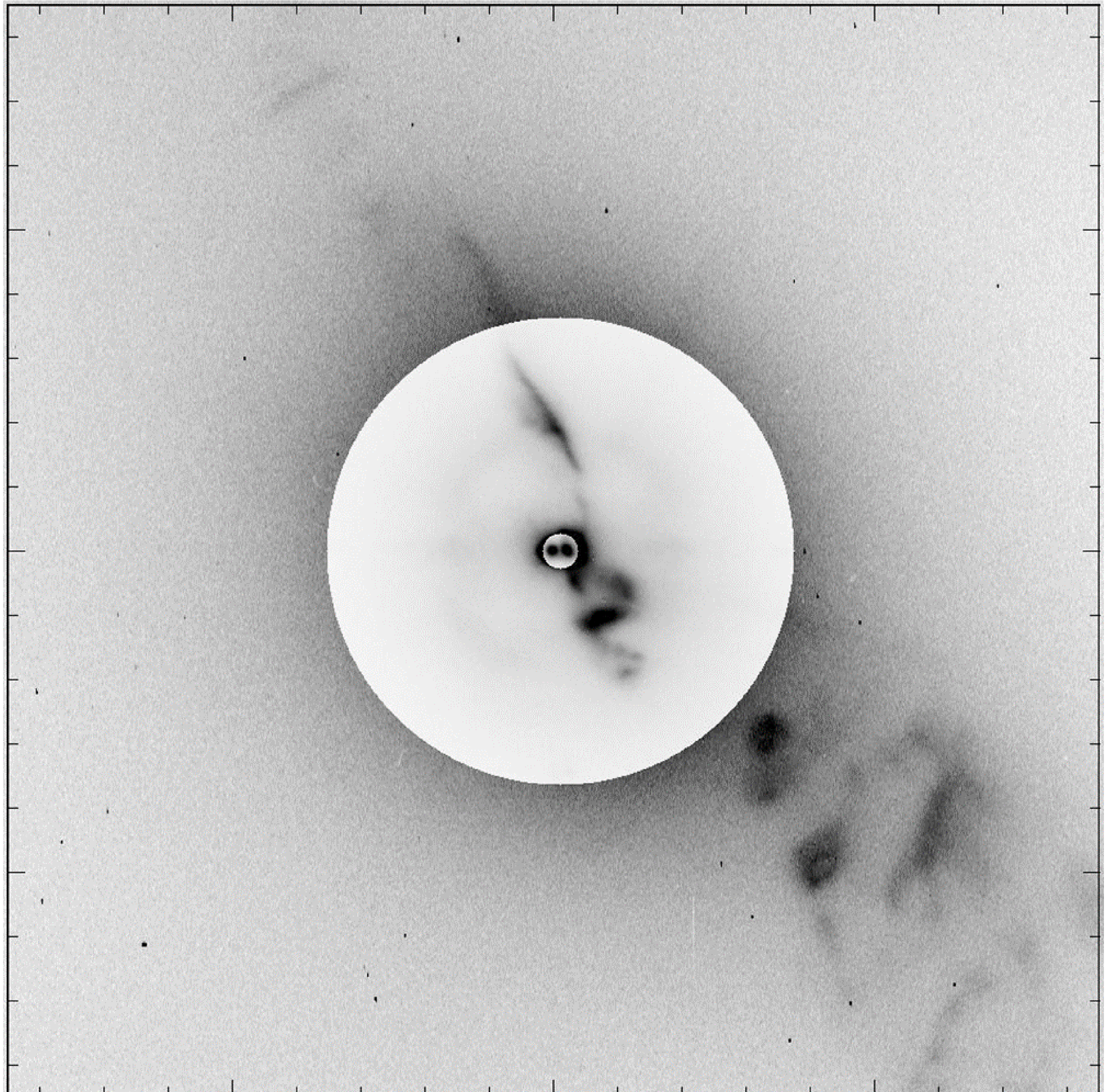

R Aqr Hα map

narrow (1nm) Hα
3.4” x 3.4”

3 grey scale regions
(linear)

binary 10-10000 cts

“inner” jet 10-1000 cts

“outer” jet 10-100 cts

Schmid et al., 2017

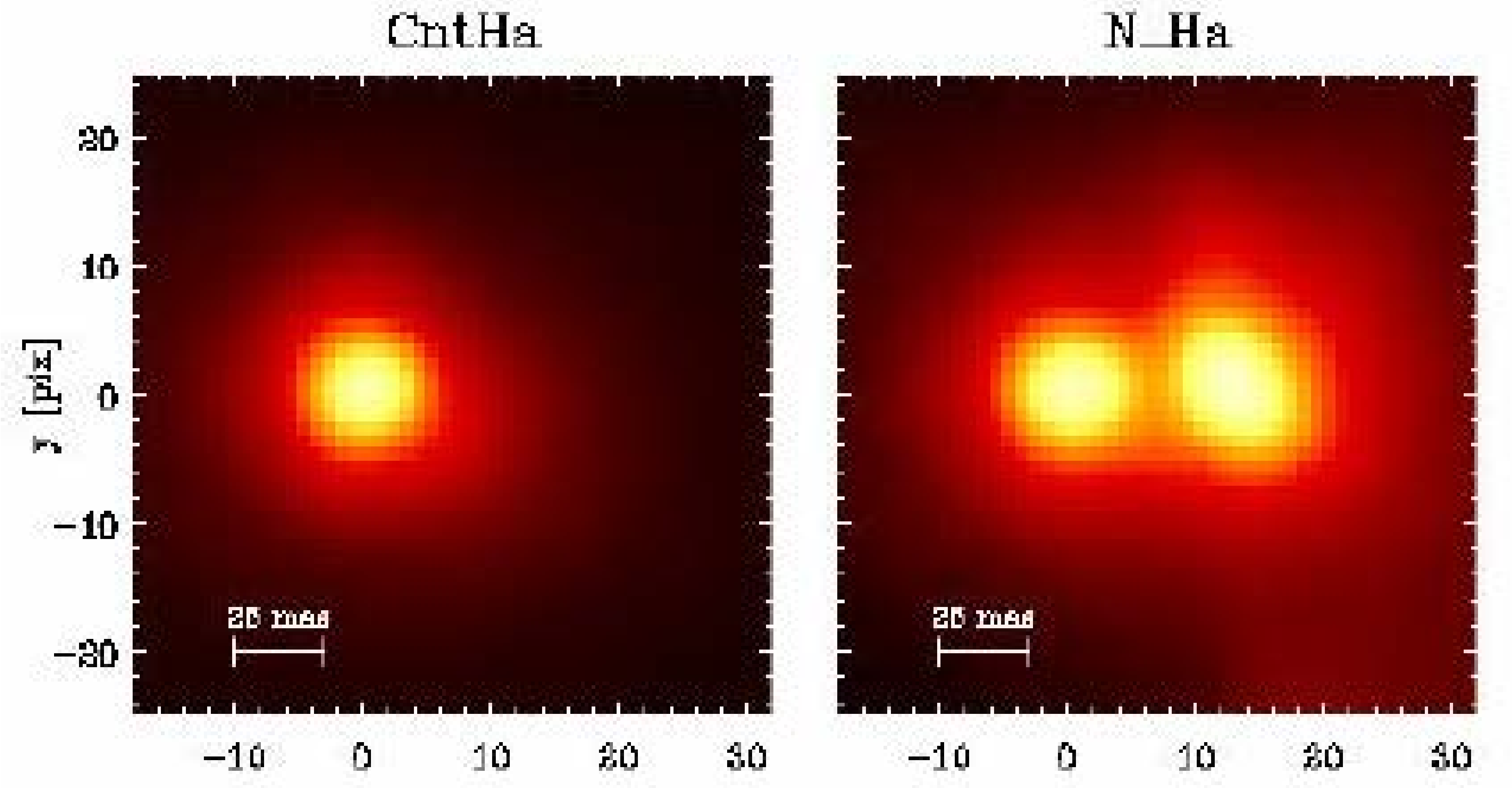

continum λ=645 nm

Halpha λ=656 nm

simultaneous image in the two ZIMPOL arms

left source: continuum of mass-losing red giant

right source: Hα of accreting companion – which produces the jets

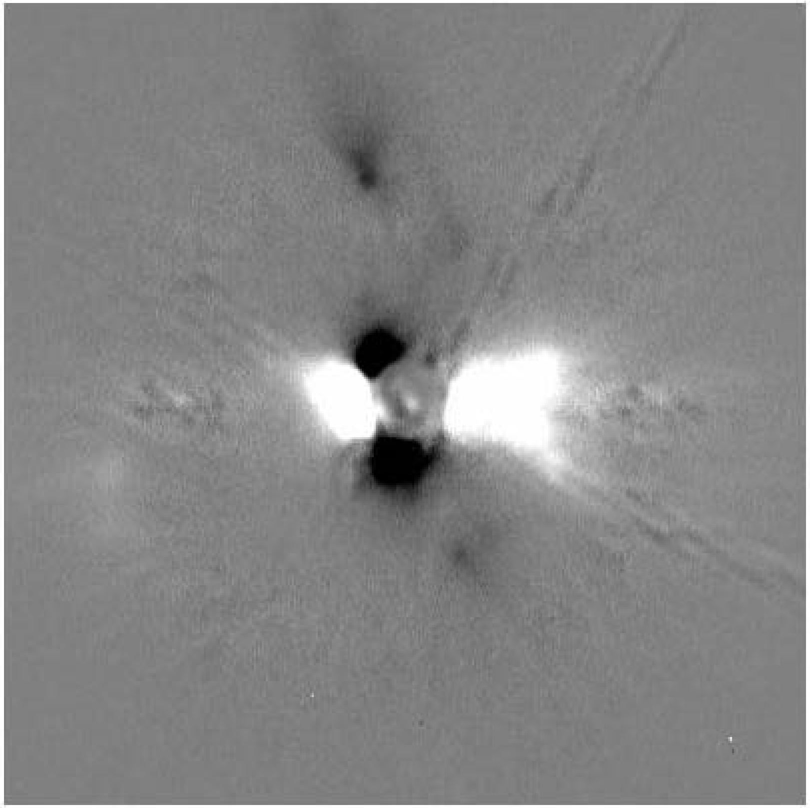

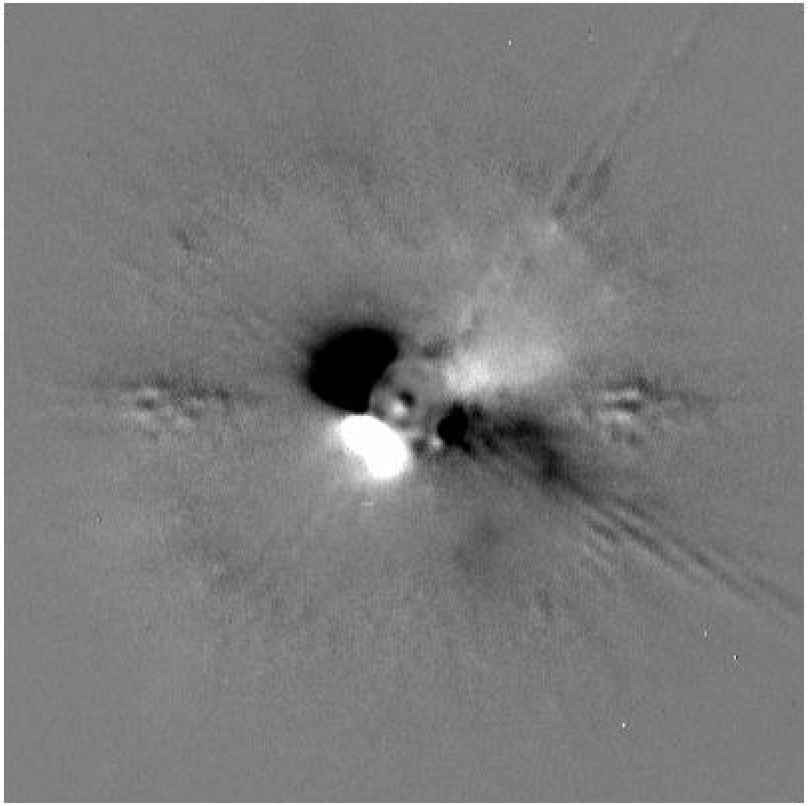

Stokes Q
$I_0 - I_{90}$

Stokes U
$I_{45} - I_{135}$

R Aqr: light scattering by the circumstellar dust within 0.3 arcsec

SPHERE/ZIMPOL PSFs

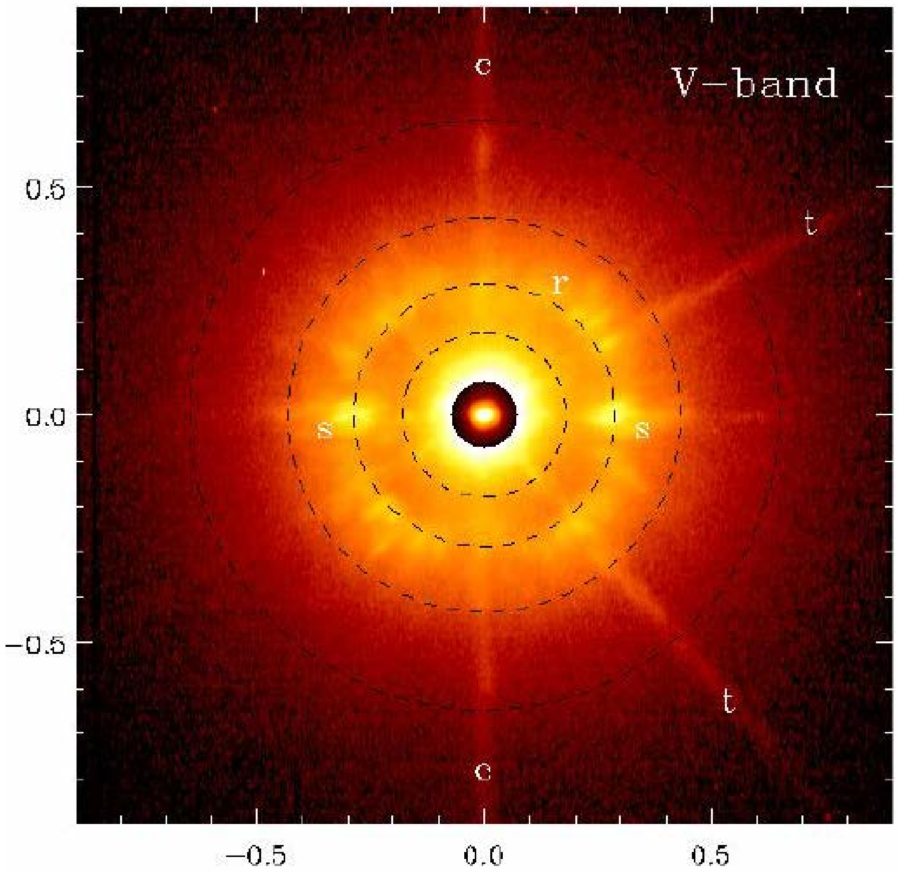

FWHM = 25 mas

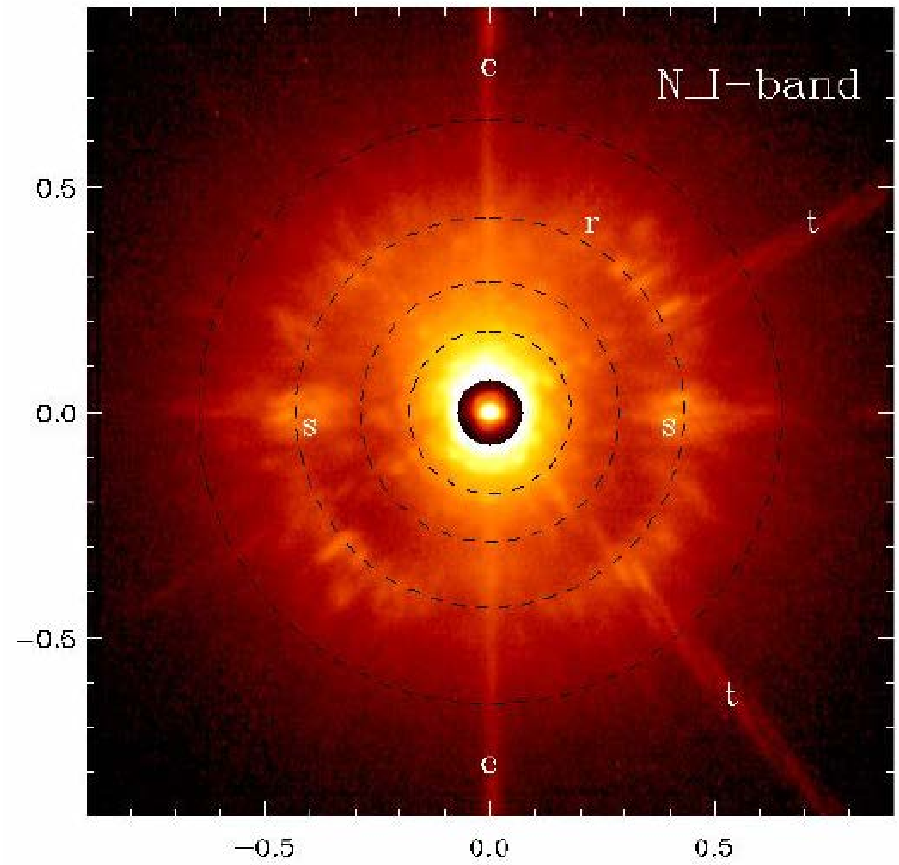

FWHM = 28 mas

Radial profiles for different atmospheric conditions

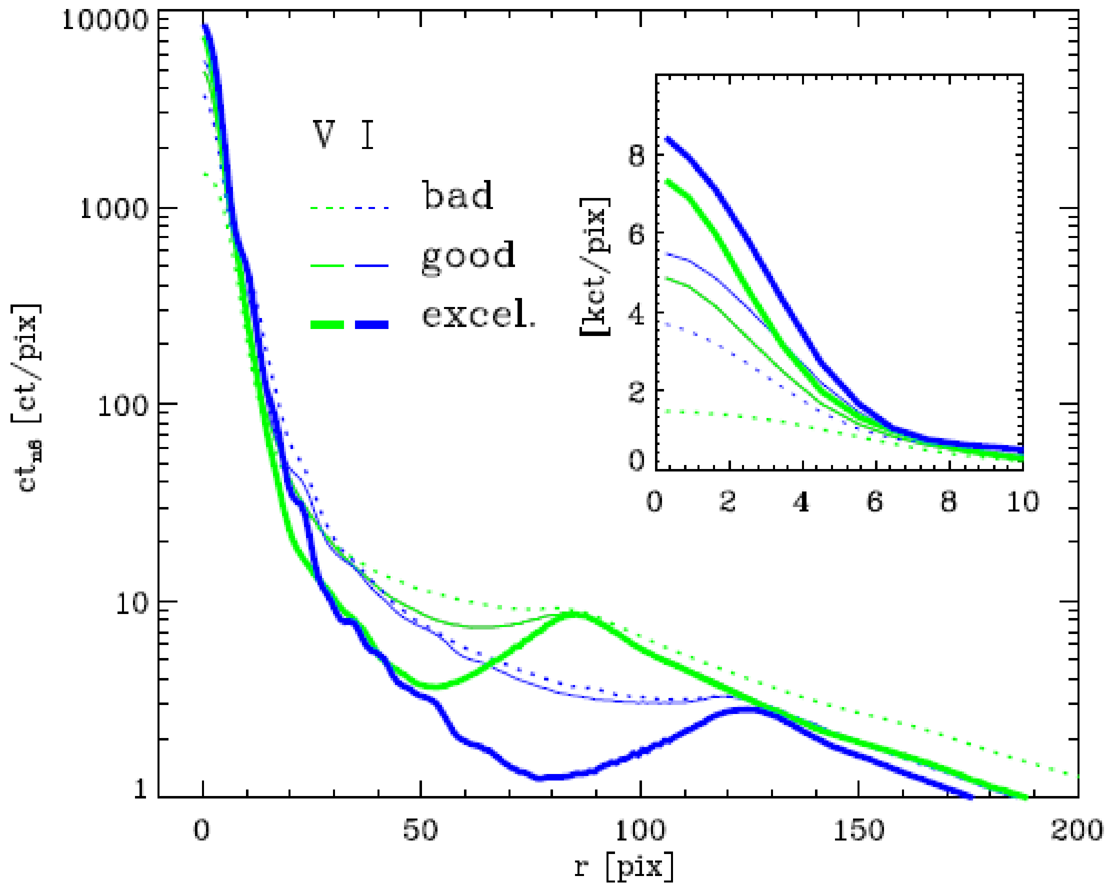

bad: seeing 1.2”

Good: seeing 0.7” (high airmass 1.7)

Excel: seeing 0.8” (bright star m=2.0)

Fig. 13. Normalized radial profiles ct_{6n} for V- and N_I-band observations of HD 161096 with “excellent” , for HD 183143 with “good”, and HD 129502 with “bad” quality PSFs.

special cases

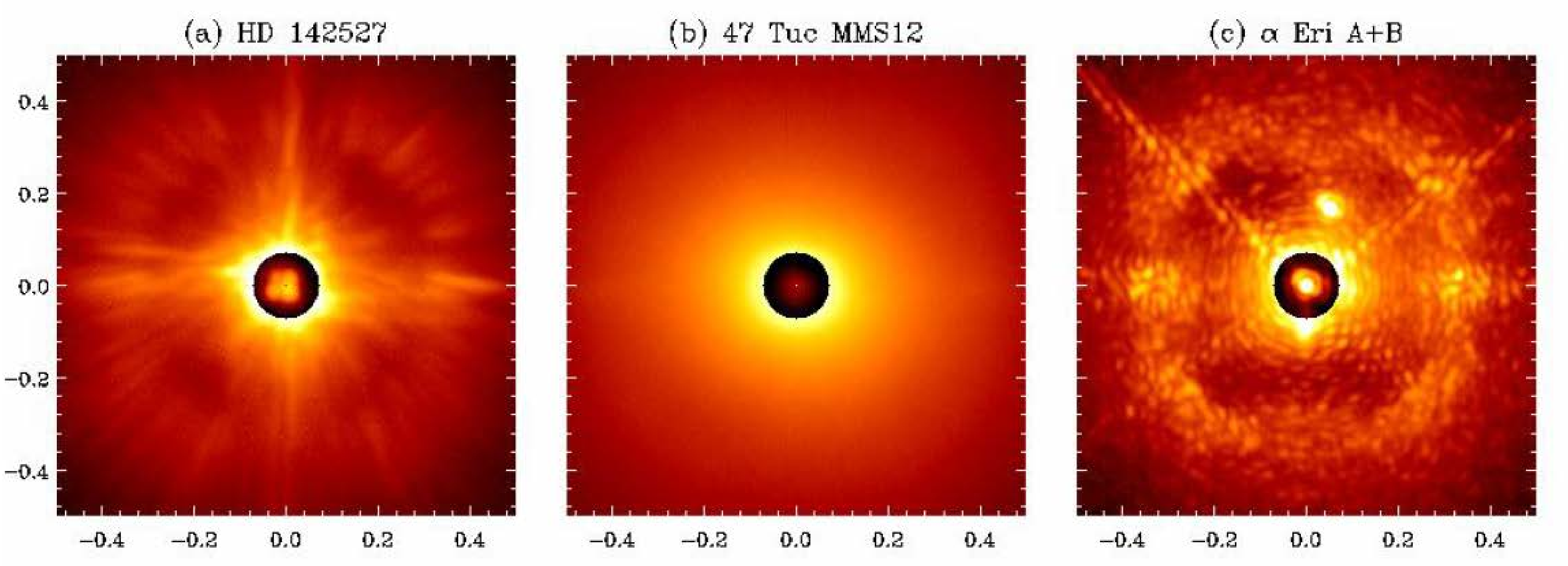

Fig. 14. Normalized PSFs for special cases: (a) VBB-filter image of HD 142527 as example for the low wind effect, (b) the faint star 47 Tuc MMS12in I_PRIM, and (c) a 10 ms snap-shot image of α Eri A and B in the line filter CntHa. The color scale is reduced by a factor of 100 for the PSF center within $r < 20$ pix.

low wind effect	faint star	snap shot
VBB-filter 3s	I_PRIM 120s	cntHa 10ms
FWHM = 54 mas	FWHM = 53 mas	FWHM=19 mas

SPHERE visual coronagraph

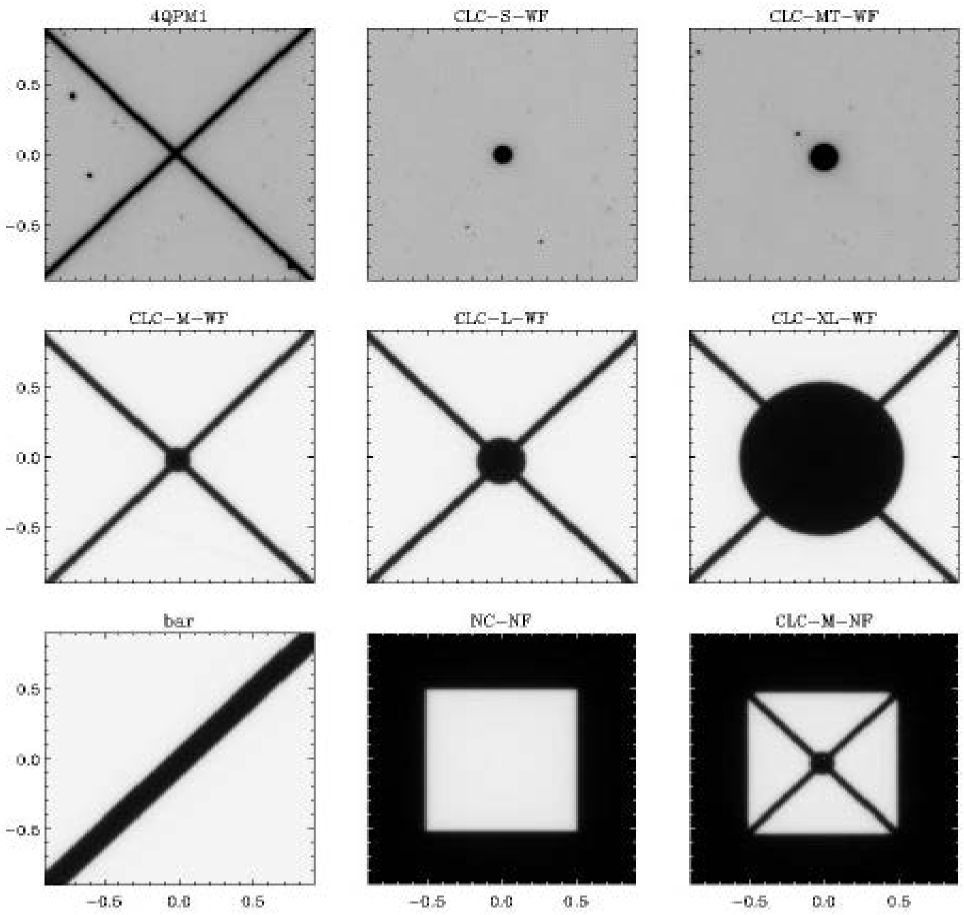

focal plane masks

Fig. 2. Images of the central part (1.8″×1.8″) of focal plane masks available in the visual coronagraph of SPHERE. The mask in the top row are deposited on a substrate and therefore the grey scale was enhanced to illustrate the frequency of dust features on the mask. The masks in the second and third row are suspended.

small IWA

different masks

- small
- medium
- 4QPM
- no mask

target α Hyi
d = 92 mas
$C_I = 4.7\ 10^{-3}$
$C_R = 2.6\ 10^{-3}$
detected in single exposures, (no ADI)

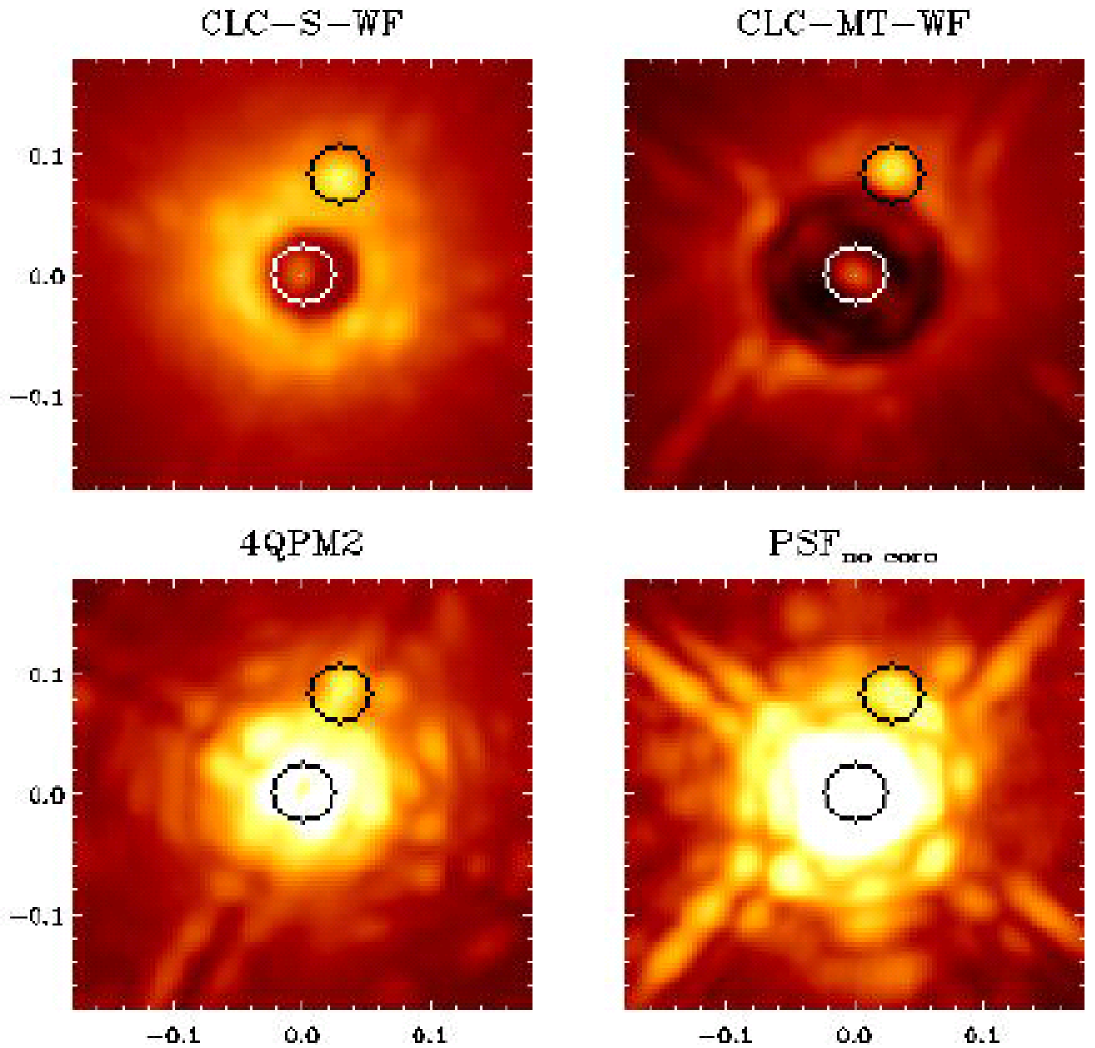

Fig. 7. *α* Hyi A and its faint companion B observed with the small S (a) and medium MT (b) classical Lyot coronagraph, the four quadrant phase mask 4QPM2 (c), and without coronagraph (d). The circles indicate the flux apertures used for component A and B.

Differential imaging

difference between
- stellar light
- target light

1) SDI: spectral (molecular bands)
2) ADI: temporal (field rotation)
3) PDI: polarimetric (scattered light)

→weak signal of target can be detected in halo of bright star

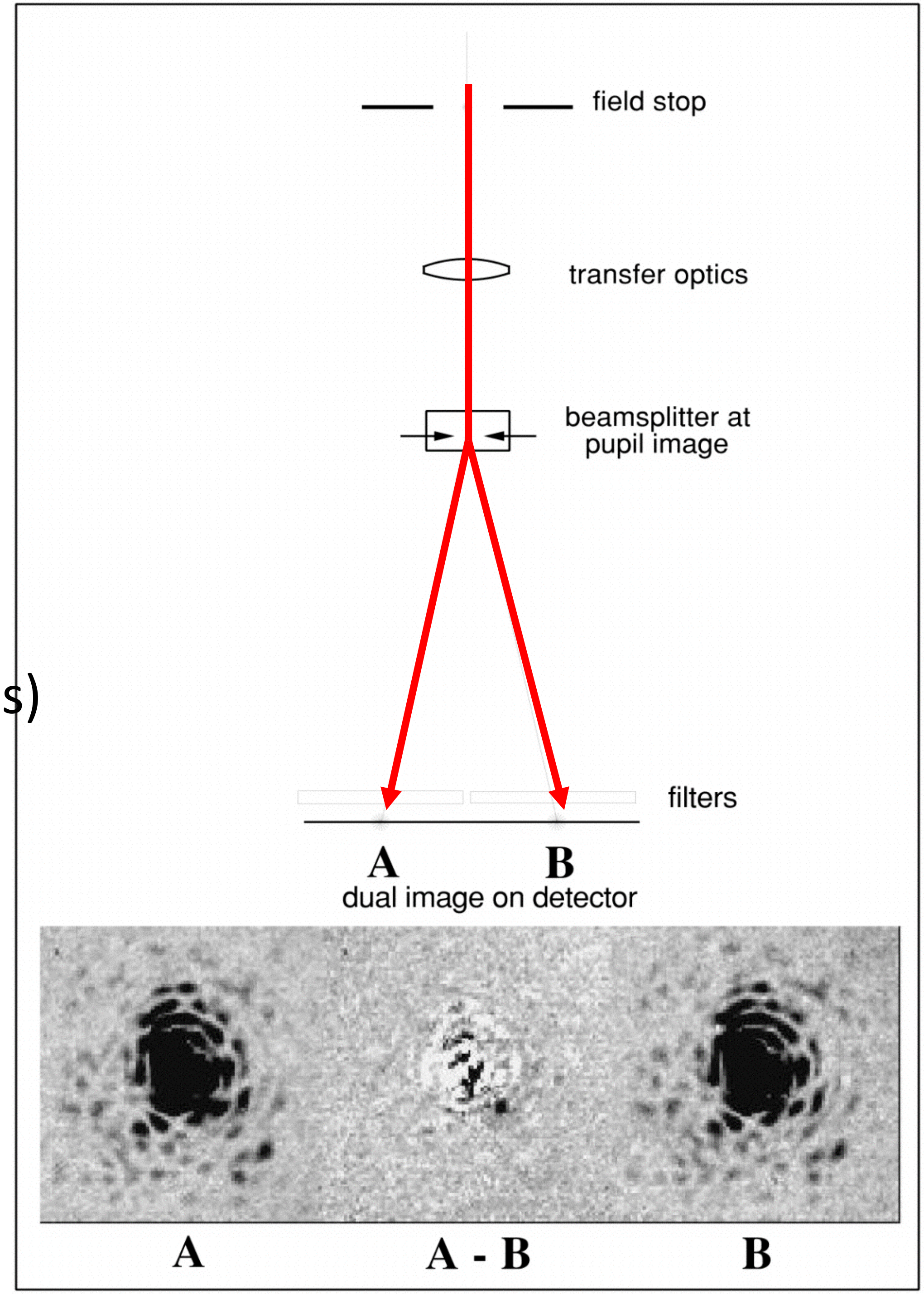

From Racine et al. 1999

ZIMPOL: polarimetric diff. imaging
basic polarimetric principle

(fast modulation)

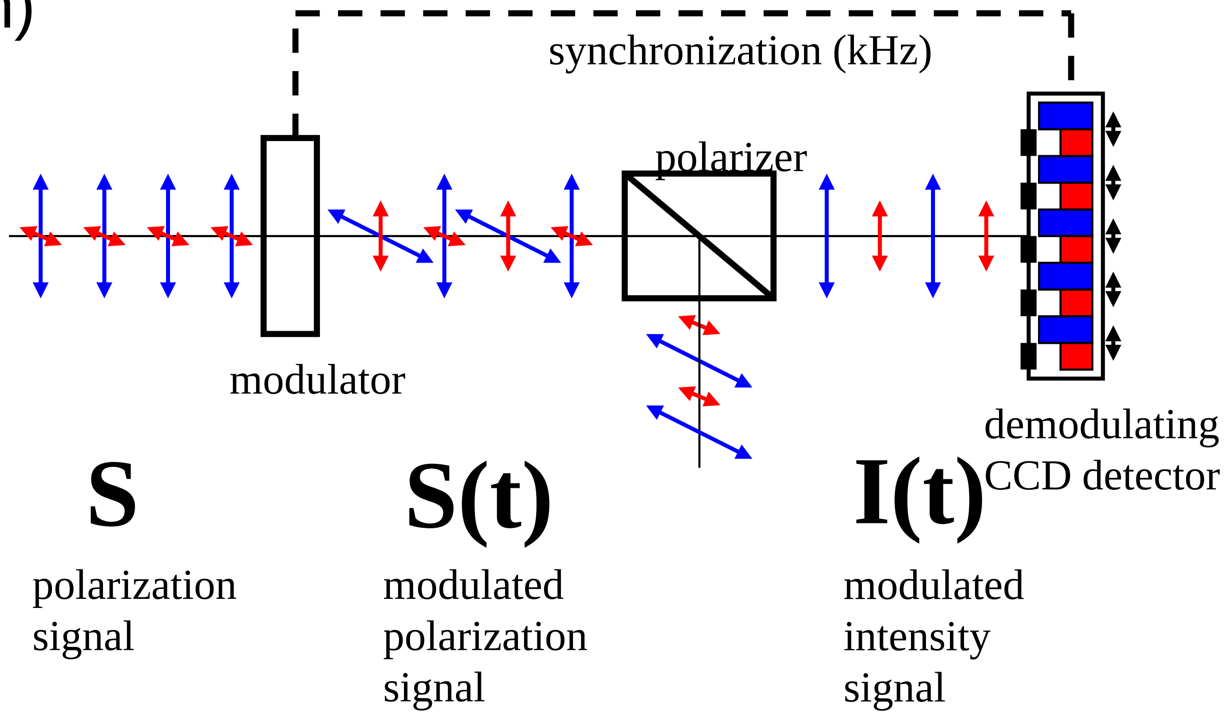

Advantages:

- images of two opposite polarization modes are created almost simultaneously
  → modulation faster than seeing variations
- both images are recorded with same pixel (buffers are different)
- both images are subject to almost exactly the same aberrations
- integration over many modulation cycles without readout (low RON)

ZIMPOL detector setup

CCD pixel – stripe mask – lens array geometry

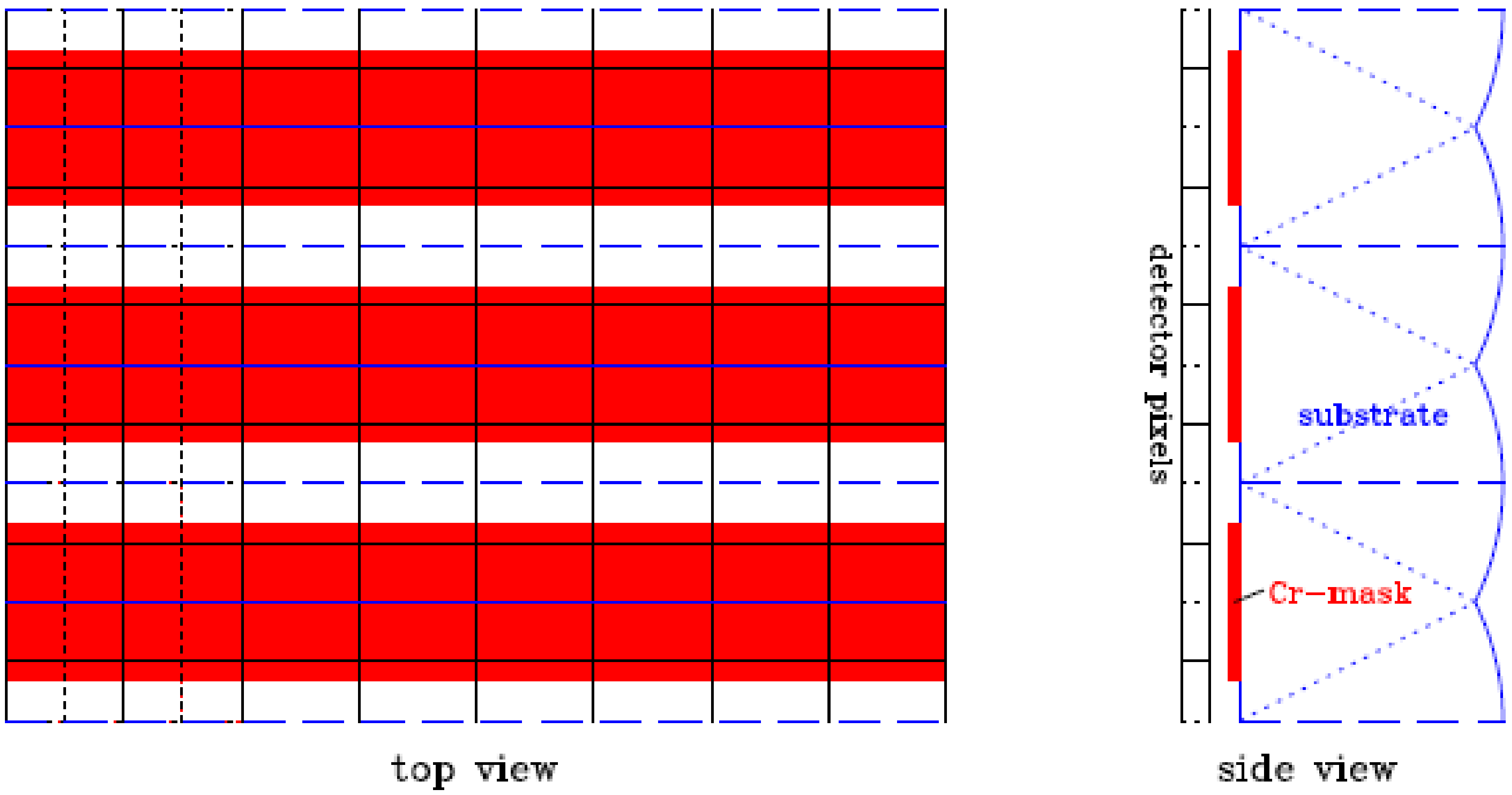

ZIMPOL “raw” image (40 x 40 pixels)

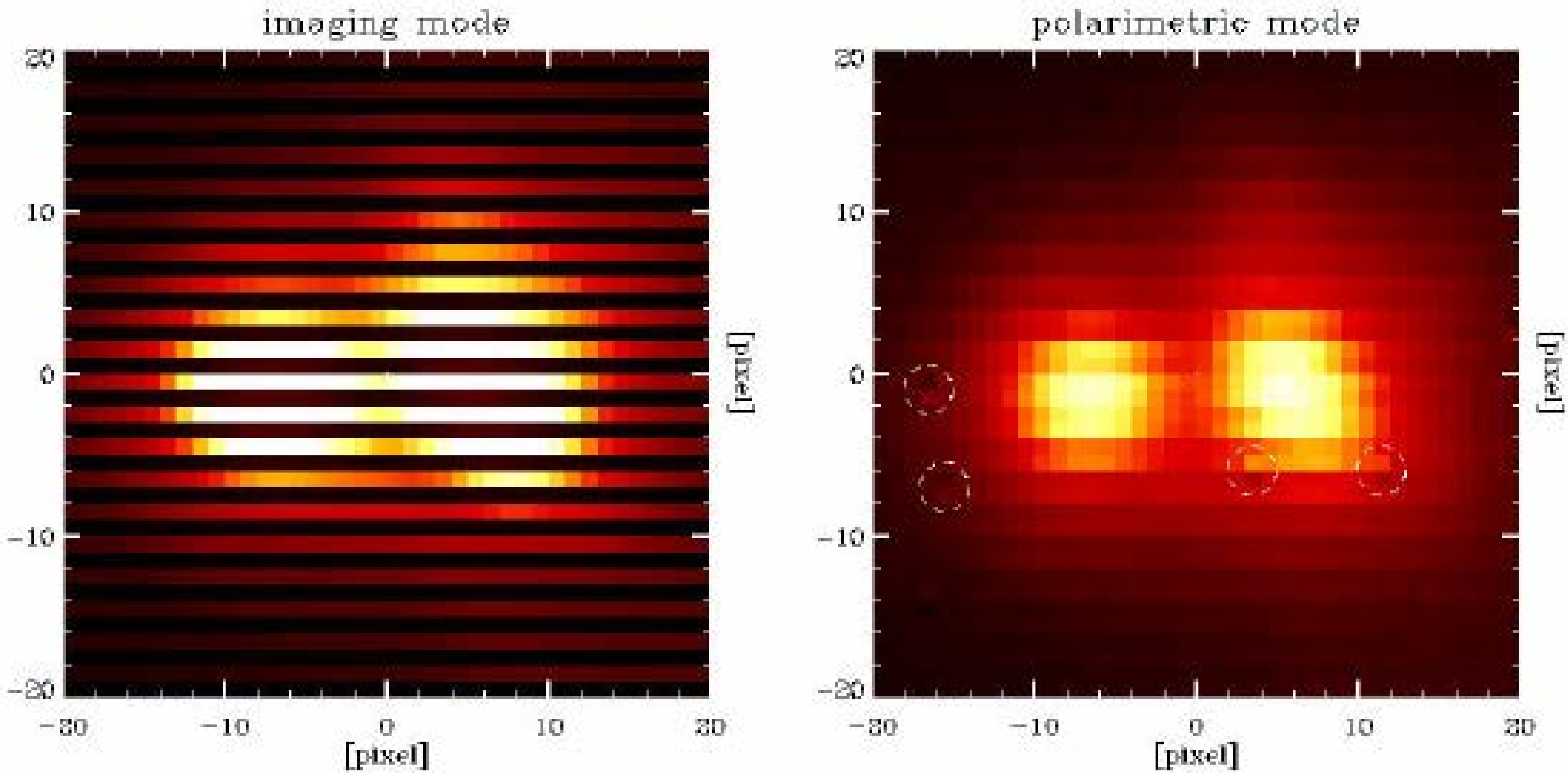

ZIMPOL polarimetry

Left: raw frame with even and odd rows with I_0 and I_{90}

Right: reduced image $Q = I_0 - I_{90}$

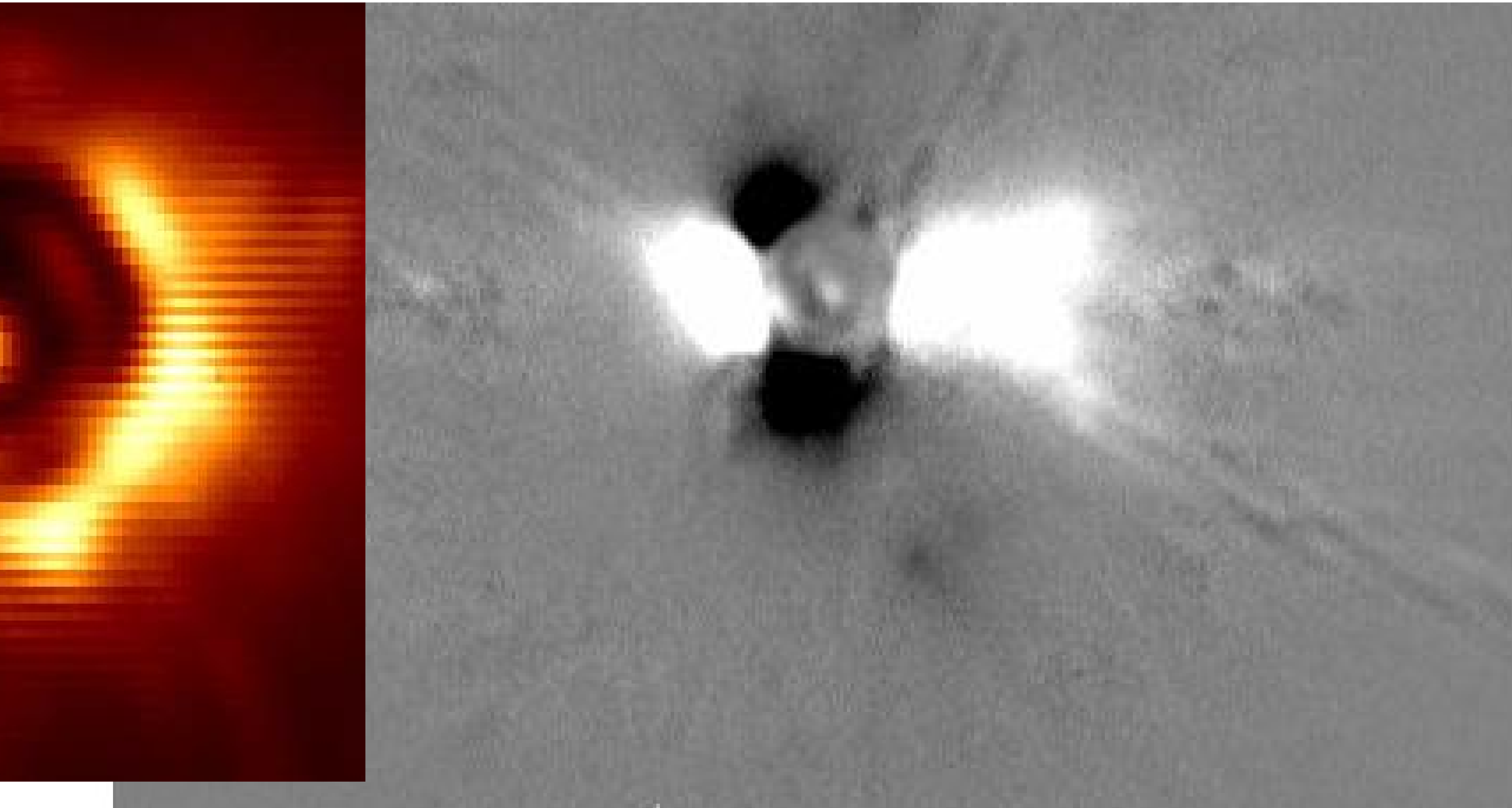

Polarimetric calibration

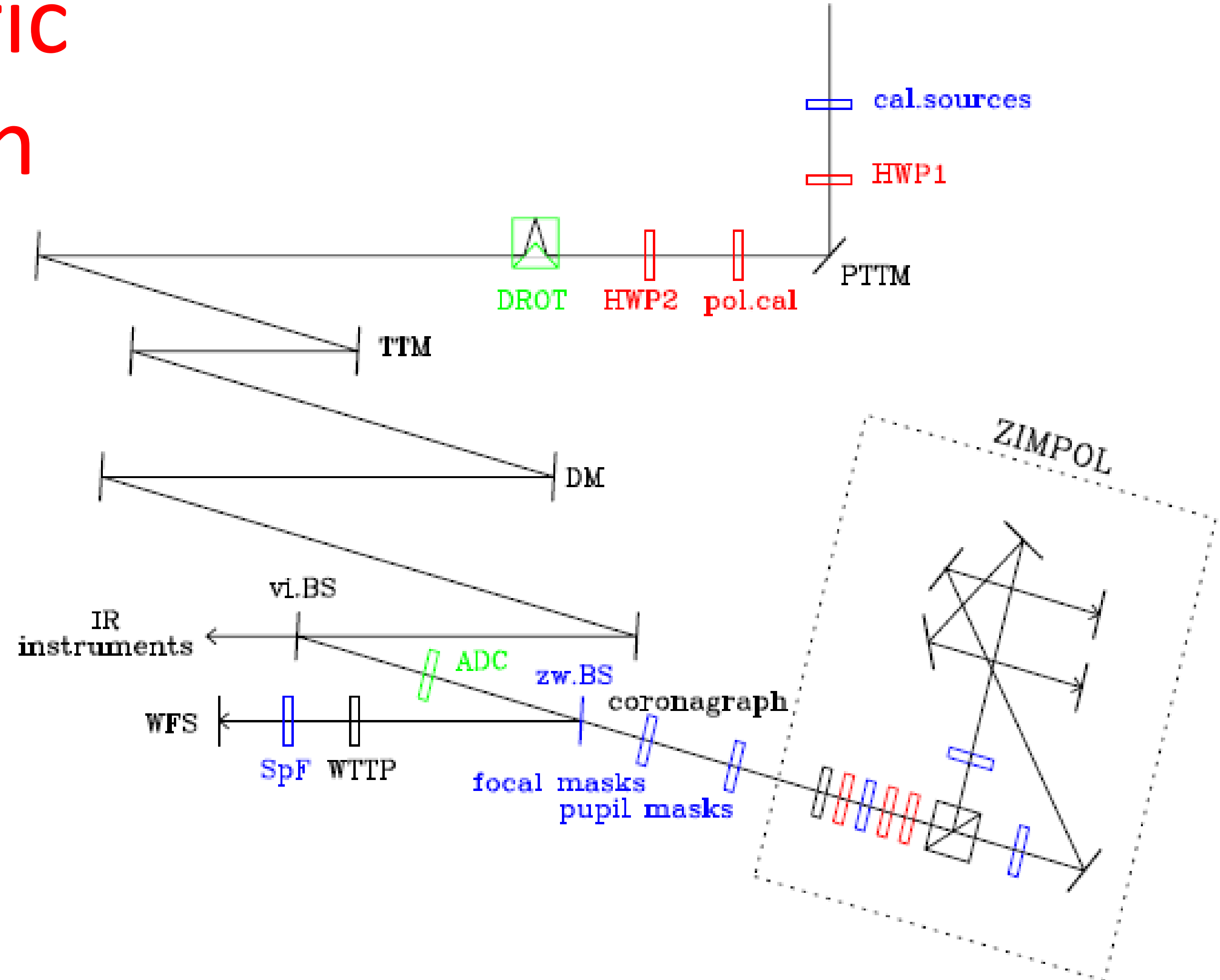

Fig. 1. Block diagram of the SPHERE common path (CPI) up to the beam splitter vi.BS and the SPHERE visual channel. The blue color indicates exchangeable components, green are rotating components, and red components are only inserted for polarimetry. The ZIMPOL box is shown in detail in Fig. 2.

ZIMPOL block diagram

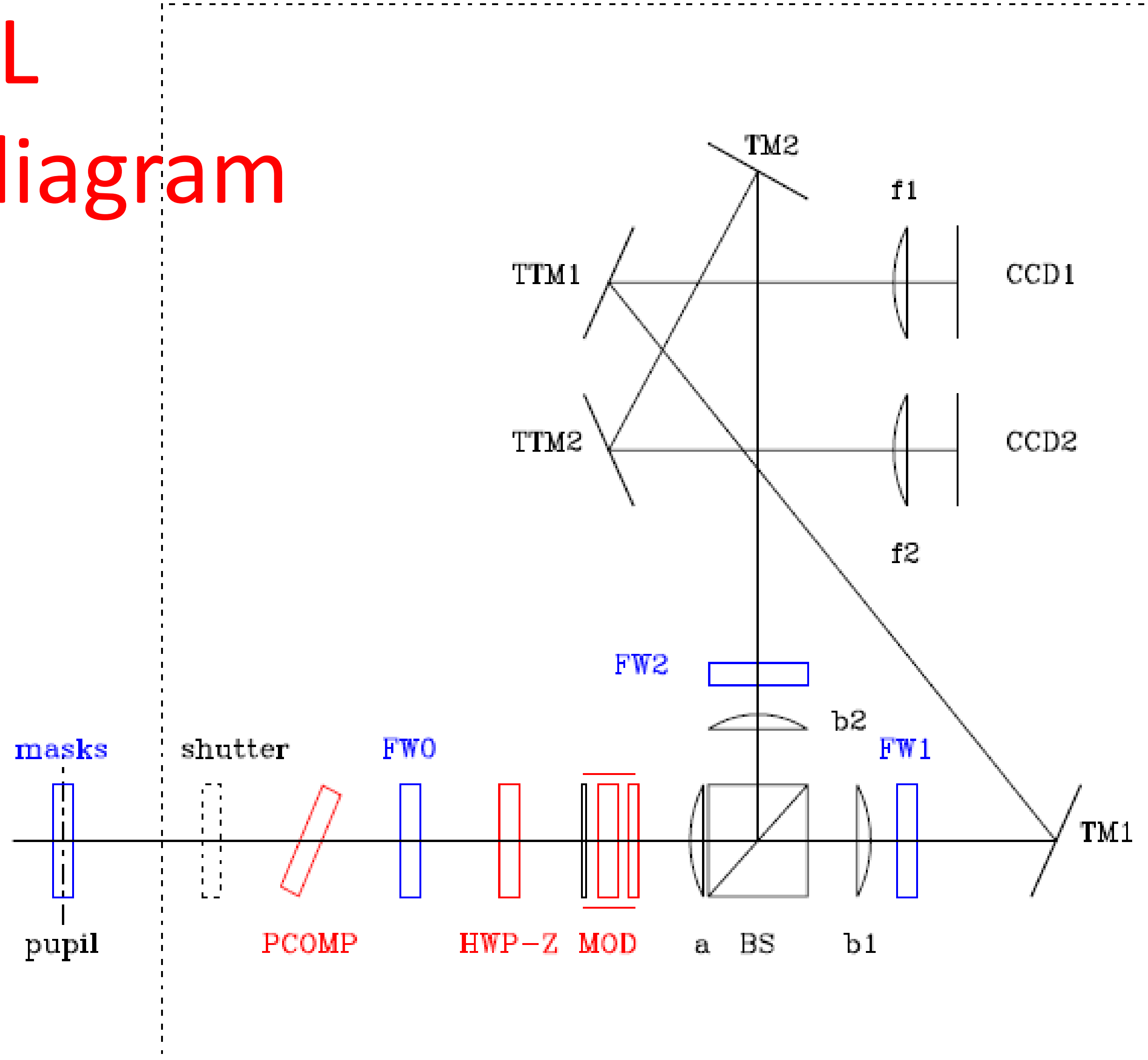

Fig. 2. Block diagram for ZIMPOL with exchangeable components plotted in blue, while red components are only inserted for polarimetry.

Residual telescope polarization

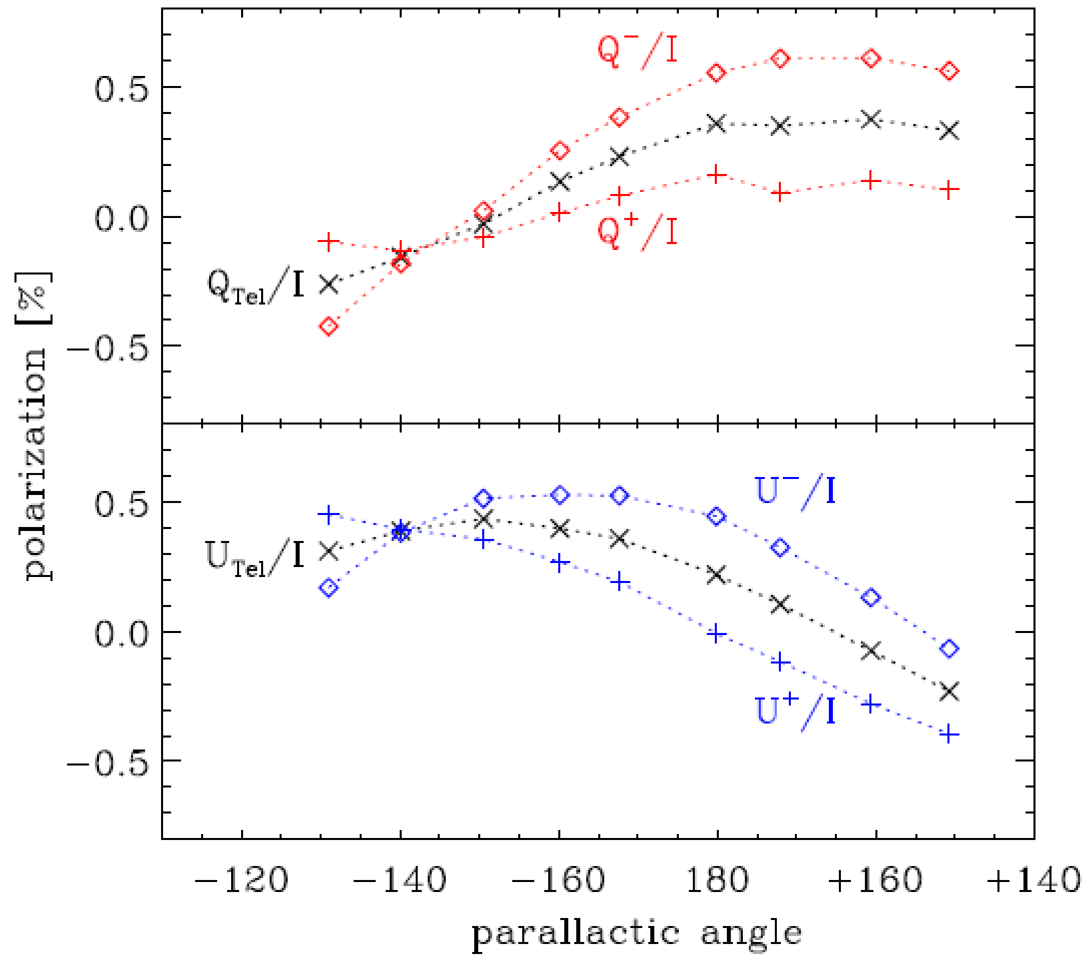

Fig. 23. Residual telescope polarization $Q_{\rm tel}/I$ and $U_{\rm tel}/I$ as function of parallactic angle for the unpolarized star ϵ Eri in the VBB band. Also shown are the individual measurements q^+, q^-, u^+, and u^- of a polarimetric cycle, which include the SPHERE/ZIMPOL instrument polarization component $\pm p_{SZ}$ for P2-mode and a field position angle offset of 60°.

Polarization orientation fixed to telescope

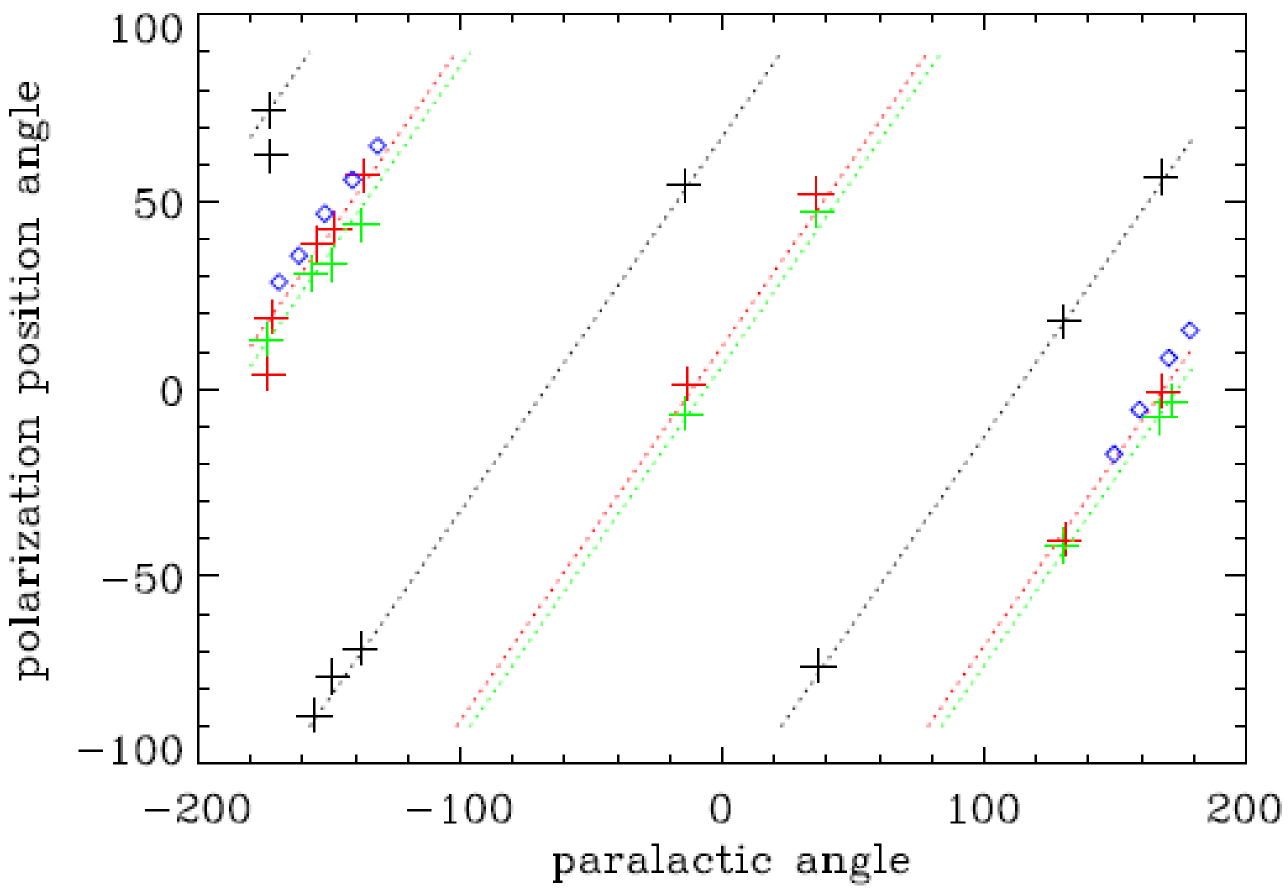

Fig. 24. Telescope polarization angle as function of the parallactic angle for zero-polarization standard stars measured in the filters V (green), N_R (red), and N_I (black). The dotted curves are best fits to the data according to Eq. 19.

Zero and high polarization standard star calibrations

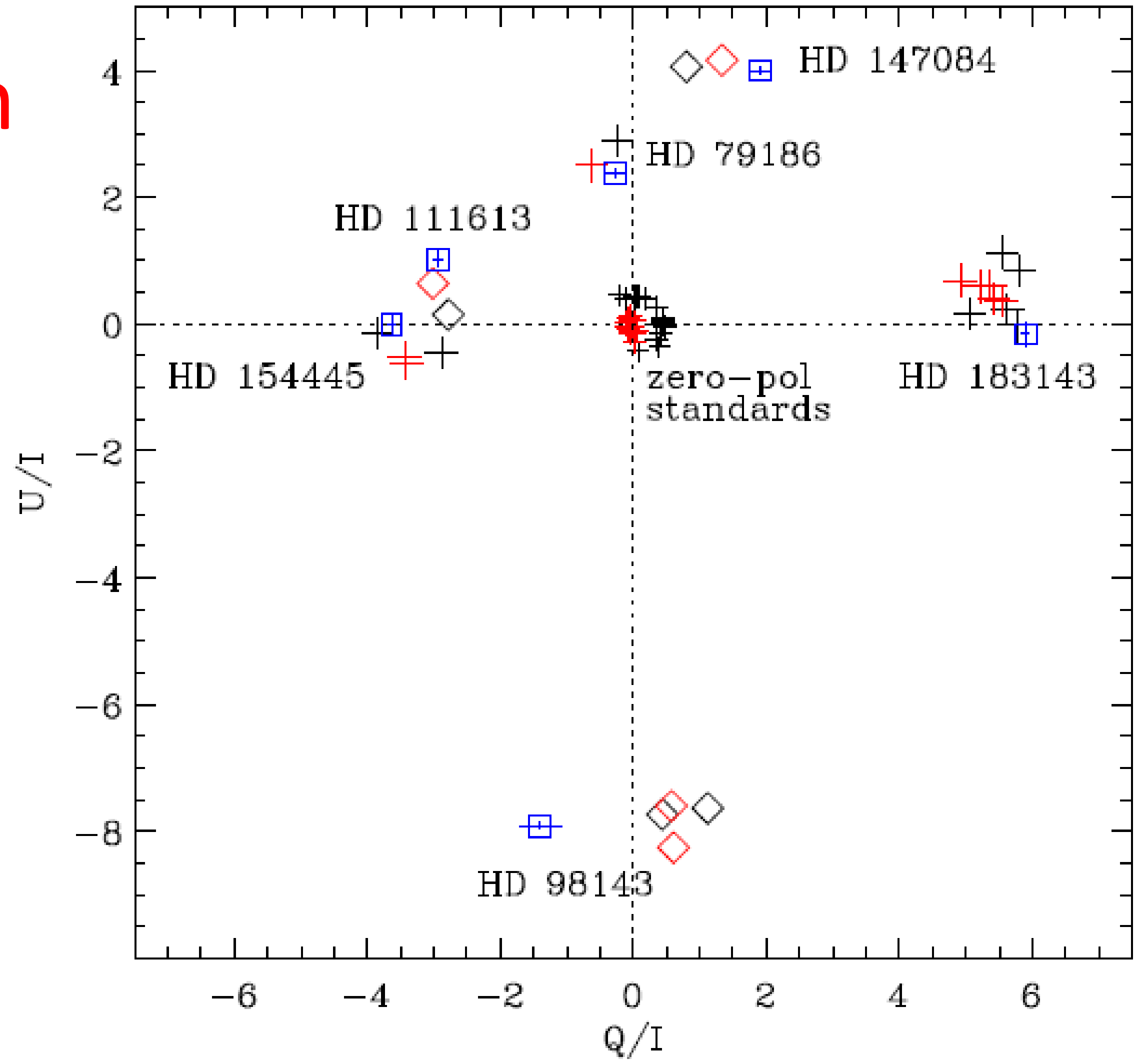

Fig. 25. Polarization of high polarization standard stars measured (c1-corrected) with ZIMPOL/SPHERE in the N_R filter (black symbols), corrected for the telescope polarization (red), and with literature values (blue) .

Polarimetric differential beam shift effect

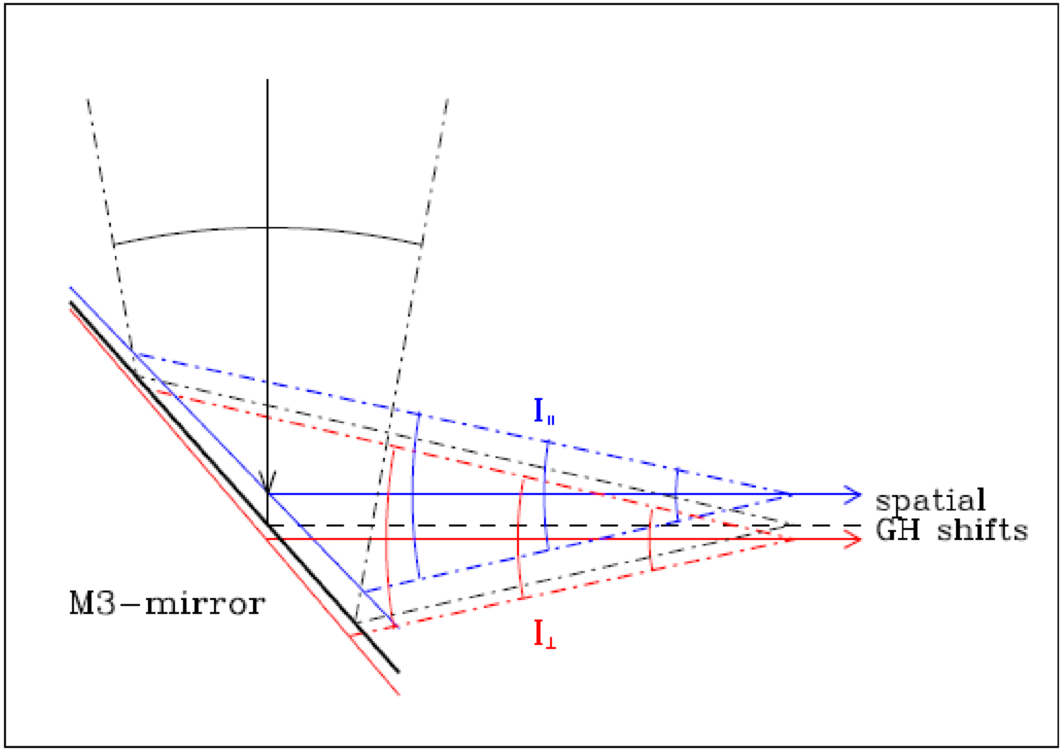

Fig. 27. Schematic and simplified illustration of the polarimetric beam shift effects for the M3 Nasmyth mirror. The incoming beam and the expected reflection according to geometric optics are plotted in black. The beam and wavefront displacements for $I_\perp$ and $I_\parallel$ caused by the phase shifts, with the corresponding "effective" mirror surface location and tilts, are hugely exaggerated and drawn in red and blue respectively.

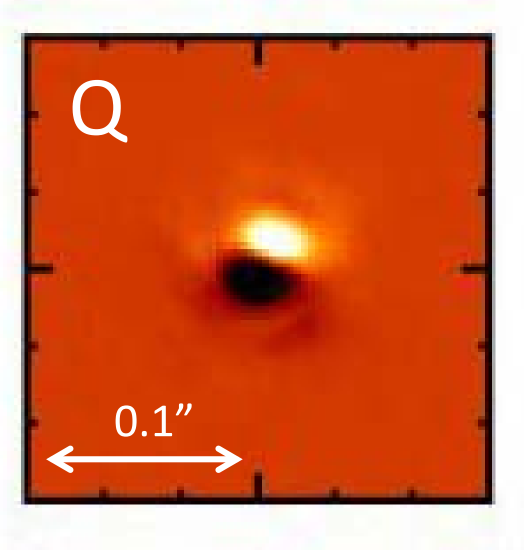

Phase shift depends on incidence angle

$$\Delta_{\perp,\parallel} = -\frac{\lambda}{2\pi}\frac{d\phi_{\perp,\parallel}}{d\theta}\bigg|_{\theta_0}$$

$$\frac{d\phi_\parallel}{d\theta}\bigg|_{45^\circ} = -0.299\,.$$

$$\frac{d\phi_\perp}{d\theta}\bigg|_{45^\circ} = 0.151$$

$$\Delta_\perp - \Delta_\parallel = 57.3\text{ nm}\,.$$

→ 0.1 mas for VLT M3

BS measurement → correction

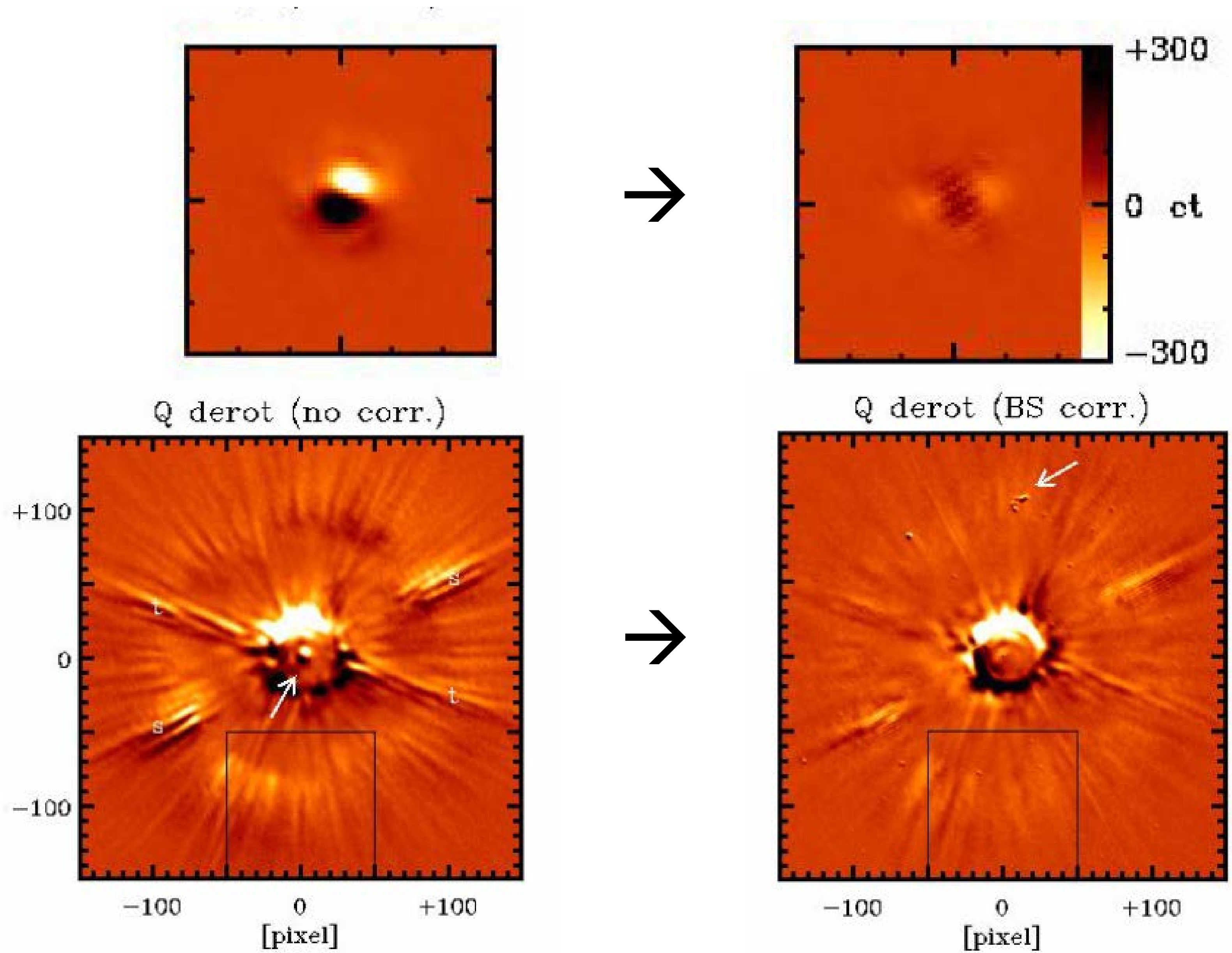

Polarimetric search for extra-solar planets

REFPLANET: SPHERE GTO-program on reflecting planets

- search for old planets around the best few target stars

$C_{pol} = f(\alpha)p(\alpha)\ R^2/d^2$, where $f(\alpha)p(\alpha) \approx 0.03\text{-}0.10$

$(R_J/AU)^2 \approx 2\ 10^{-7}$

$\approx 10^{-8}$

- set scientifically useful non-detection limits
  - for best targets: α Cen A +B, Sirius, ε Eri, Altair, τ Cet
  - for systems with known planets: Prox b, Gl 876 b

- investigate the limitations of the ZIMPOL technique (preparation for a planet finder camera for the E-ELT)

Expected polarization

- for Rayleigh scattering by molecules or haze particles

→ strong phase dependence expected:

inclination = 0°

p=constant & high

pos. angle rotates

inclination = 70°

p=high for large separation

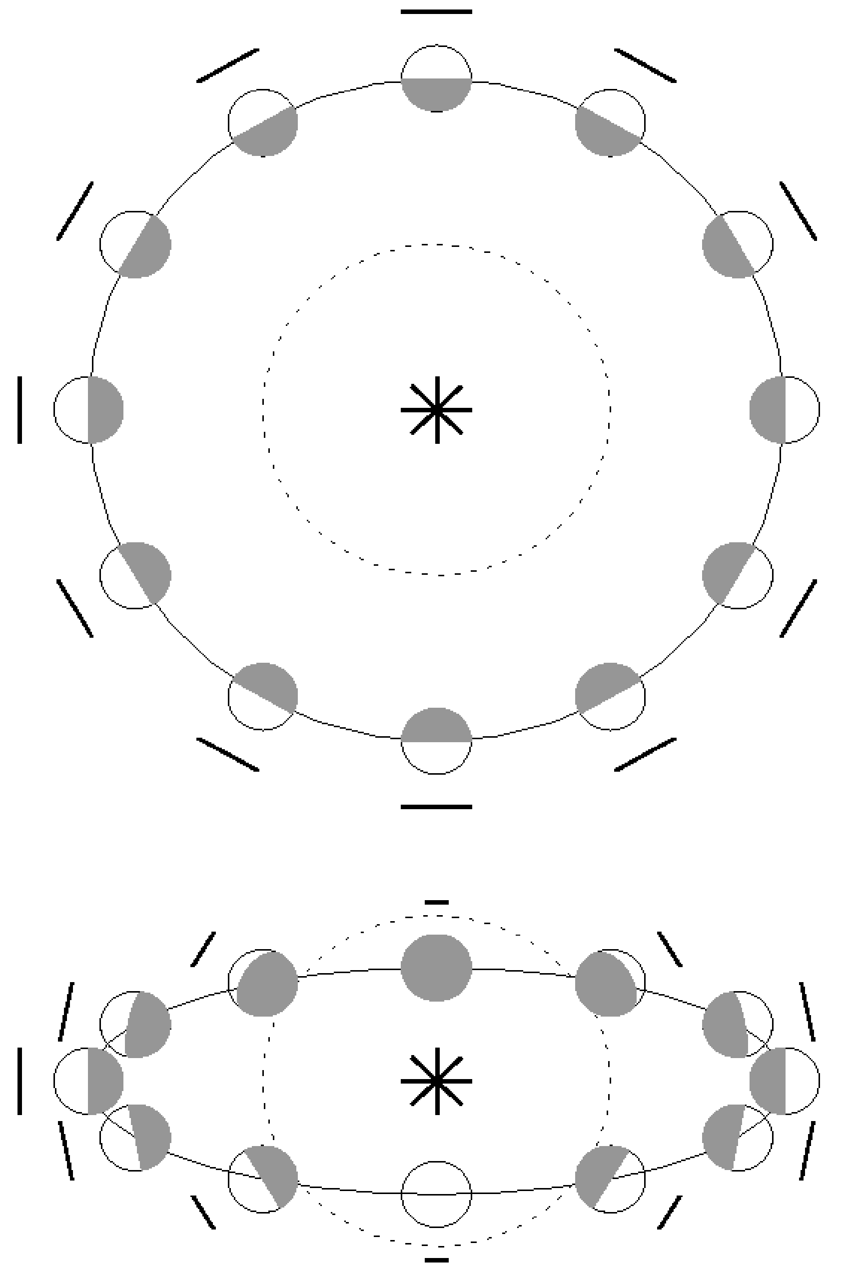

Single Rayleigh scattering

- 100% pol. for 90^o scattering angle
- Forward and backward scattering enhanced but unpolarized

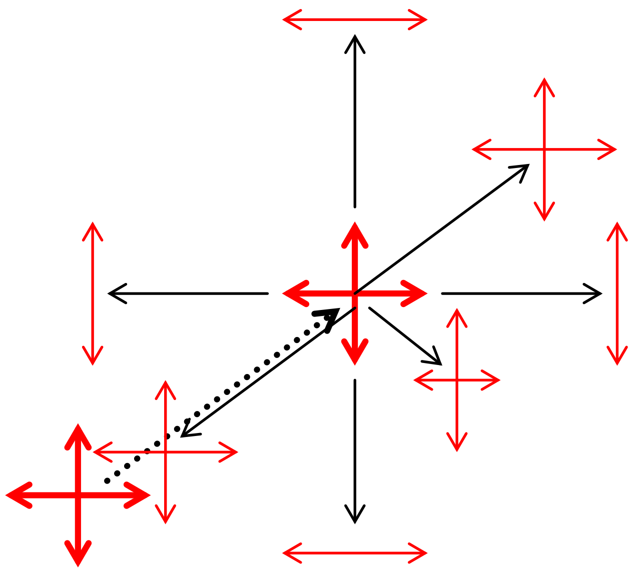

Dust scattering: $a < \lambda$ -- like Rayleigh scattering

$a > \lambda$ -- polarization direction like Rayleigh

-- p_{max} reduced

-- plus strong diffraction (forward dir.)

Contrast limit reached up to now

5 sigma point source detection limit
for Q-frame of very good half night (2h)
0.2"-0.4": ~3 10^{-7} ($\Delta=16.3^{m}$)
0.6"-0.8": ~3 10^{-8} ($\Delta=18.8^{m}$)
> 1.0": ~1 10^{-8} ($\Delta=20^{m}$)

about a factor of 10 above $3R_E$ planet

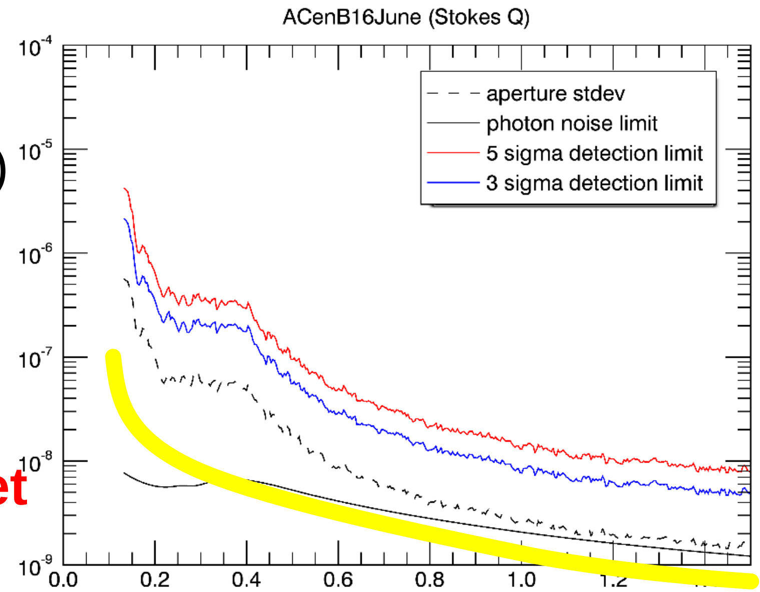

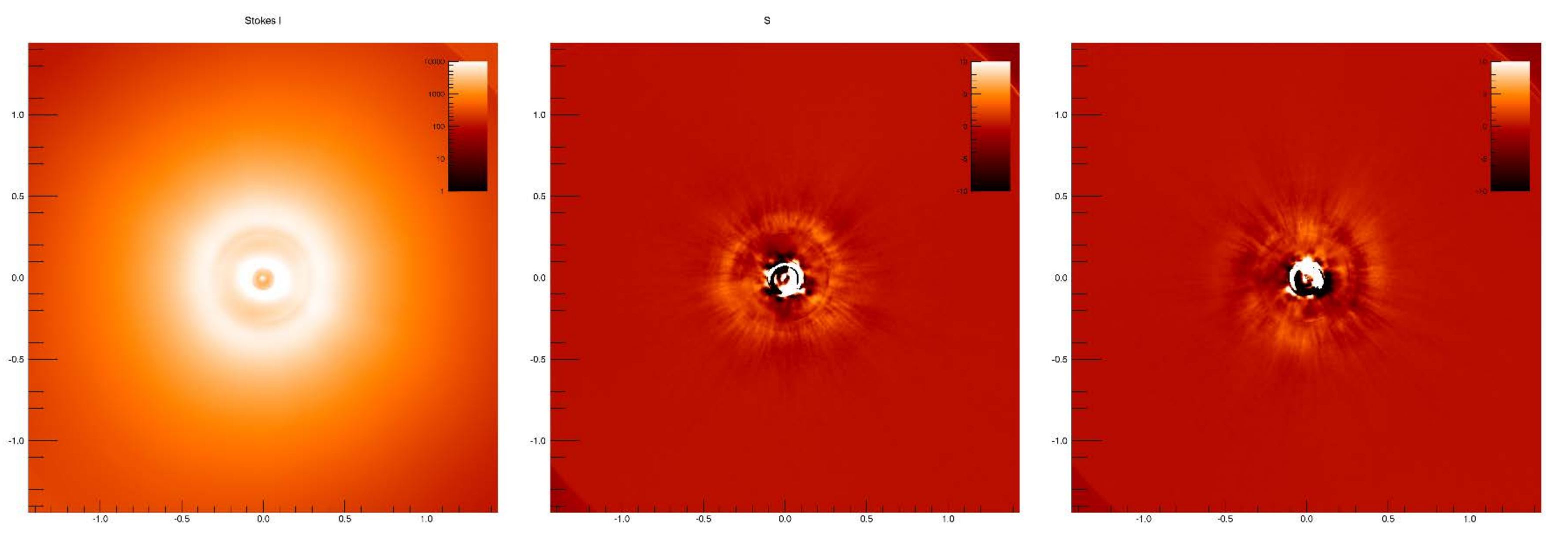

Pupil optimization with a binary amplitude mask

study by Polychronis Patapis

supress 1st diffraction ring with a reshaped pupil

Tuned for two targets

-Prox b, sep: 0.38 mas

-Gl 876 b, sep: 44 mas

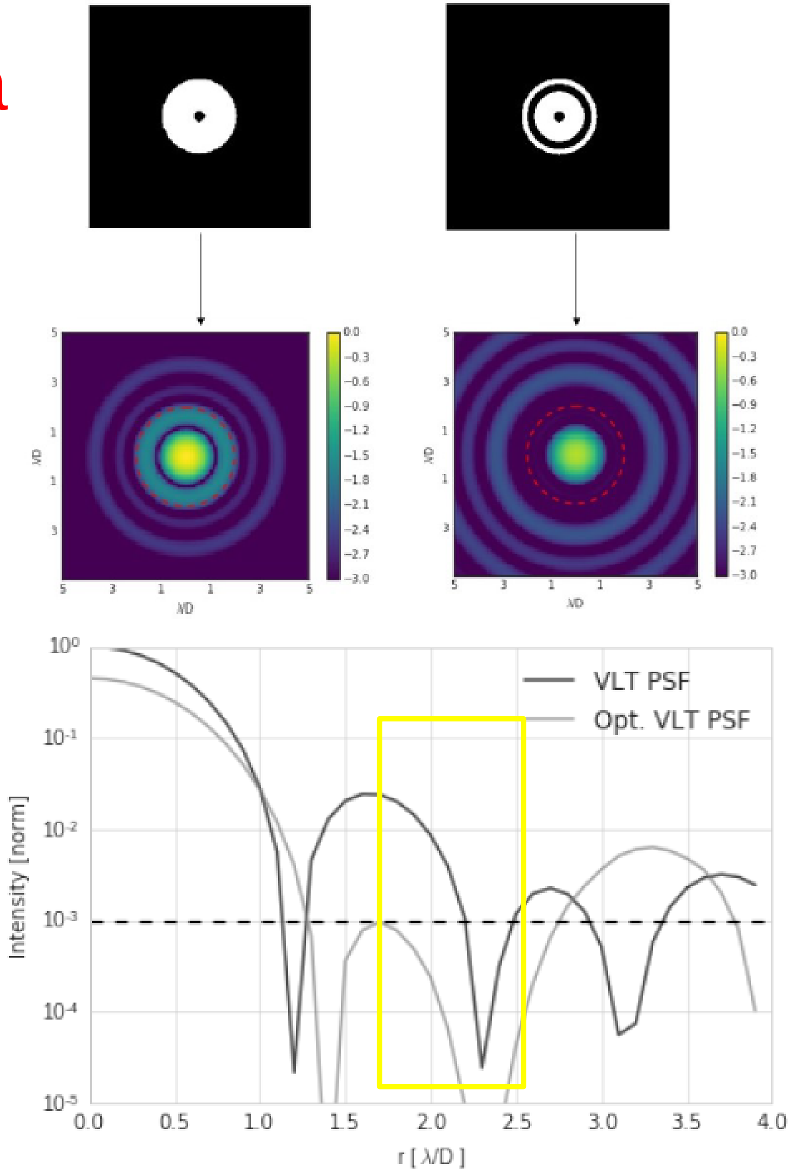

Figure 1.4: Simulation of monochromatic (750 nm) case. Top Left: VLT pupil and PSF in log scale (min=10^{-3}, max=1). Top Right: Optimized pupil PSF in log scale (min=10^{-3}, max=1) after 400 iterations of the algorithm with a ring width of 20% of the aperture radius. Bottom: Azimuthal average of the intensity (log scale) versus radial separation for nominal and optimized PSF. The optimized mask produces 410^{-2} less light in the region of interest.

A 599, A16 (2017)

Lovis et al. (2017)

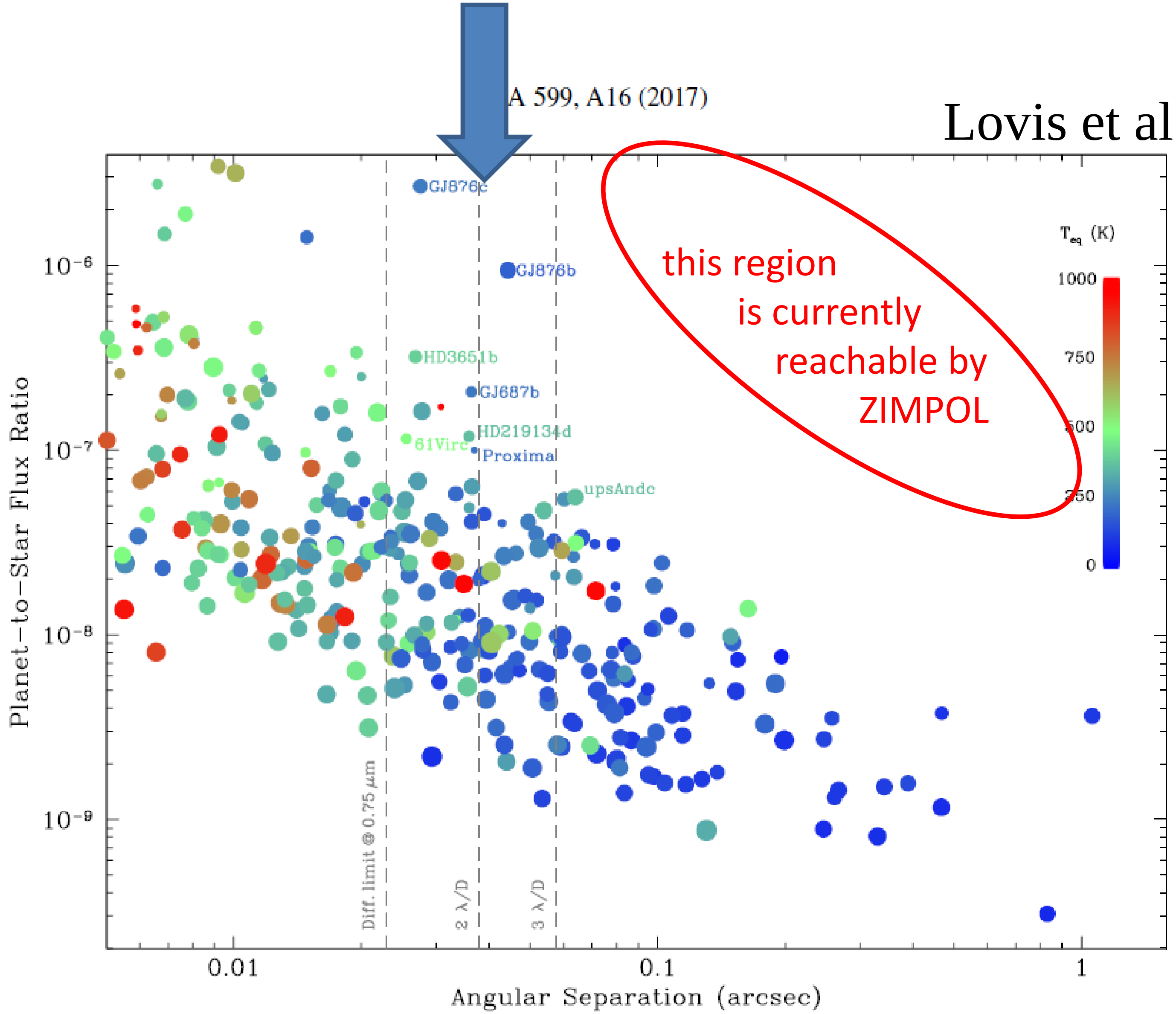

Fig. 1. Estimated planet-to-star contrast in reflected light for known exoplanets as a function of angular separation from their host star. Dot size is proportional to the logarithm of planet mass, while the color scale represents equilibrium temperature (assuming a Bond albedo of 0.3). Vertical dashed lines indicate the diffraction limit, 2 λ/D and 3 λ/D thresholds for the 8.2-m VLT at 750 nm (corresponding to the O_2 A-band).

Scattered light from circumstellar disks

DPI data with SPHERE/ZIMPOL

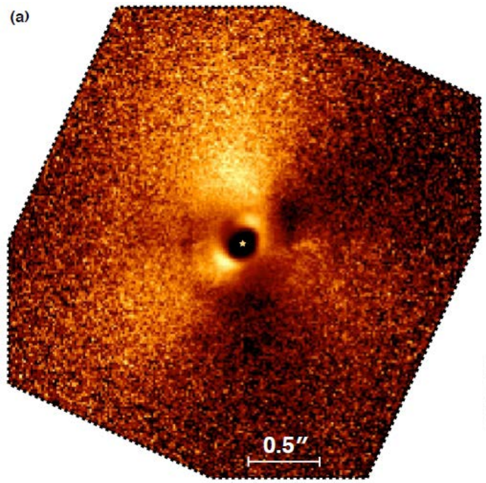

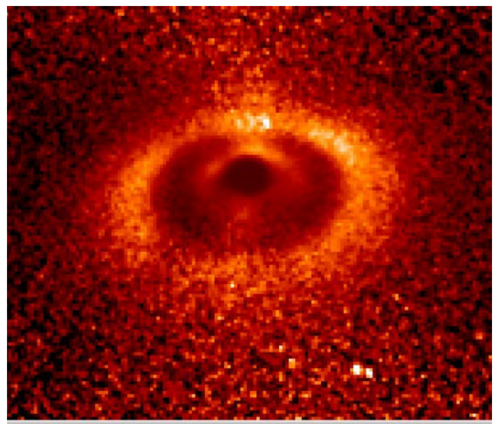

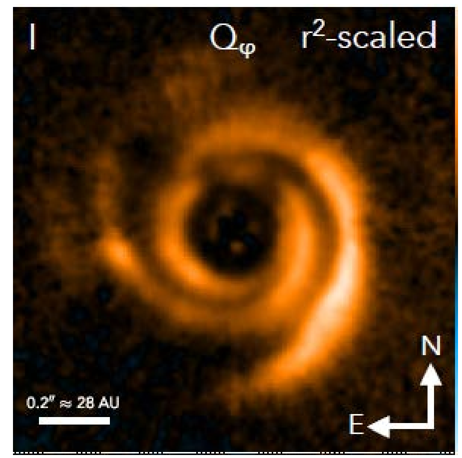

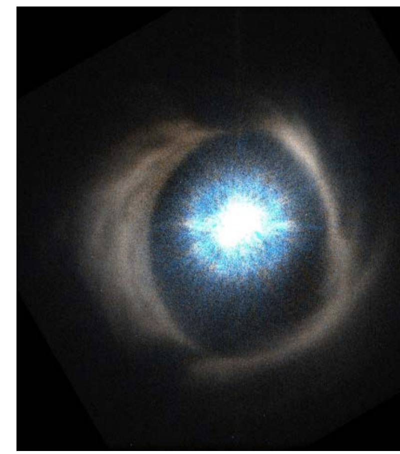

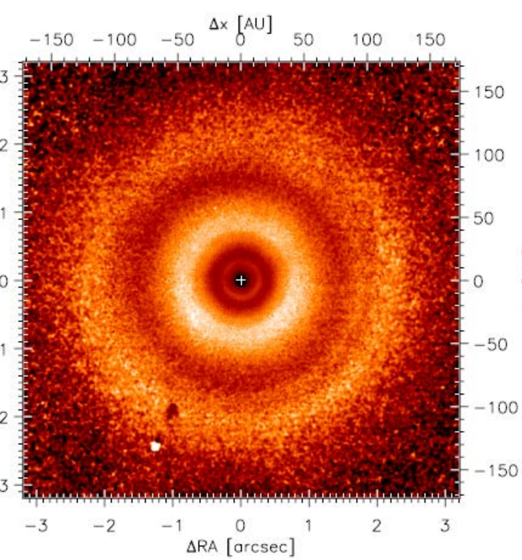

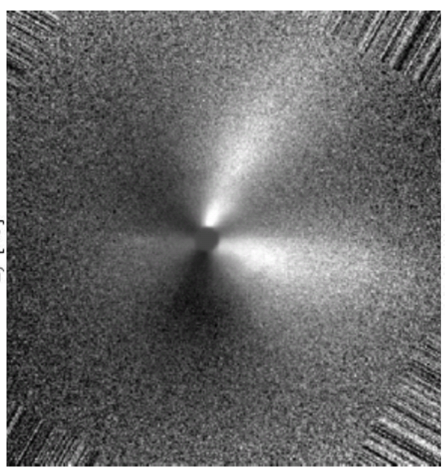

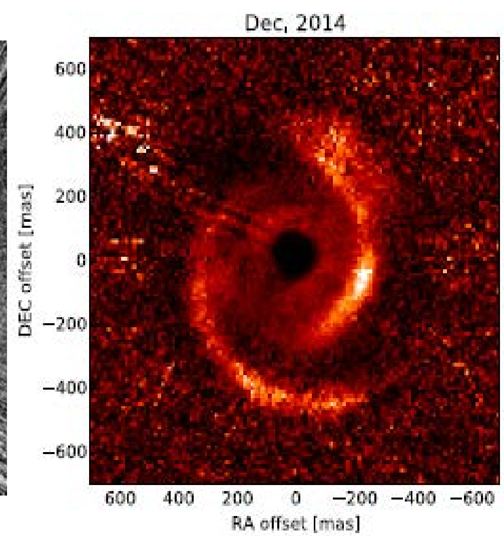

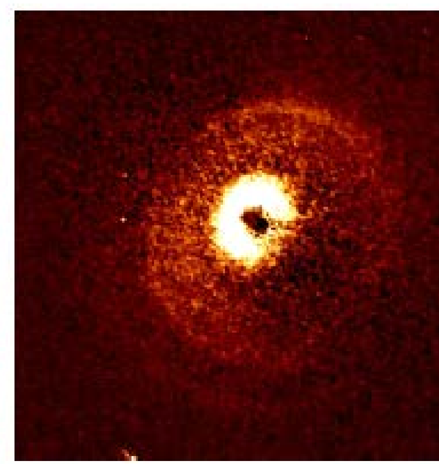

Differential polarimetric imaging of disks

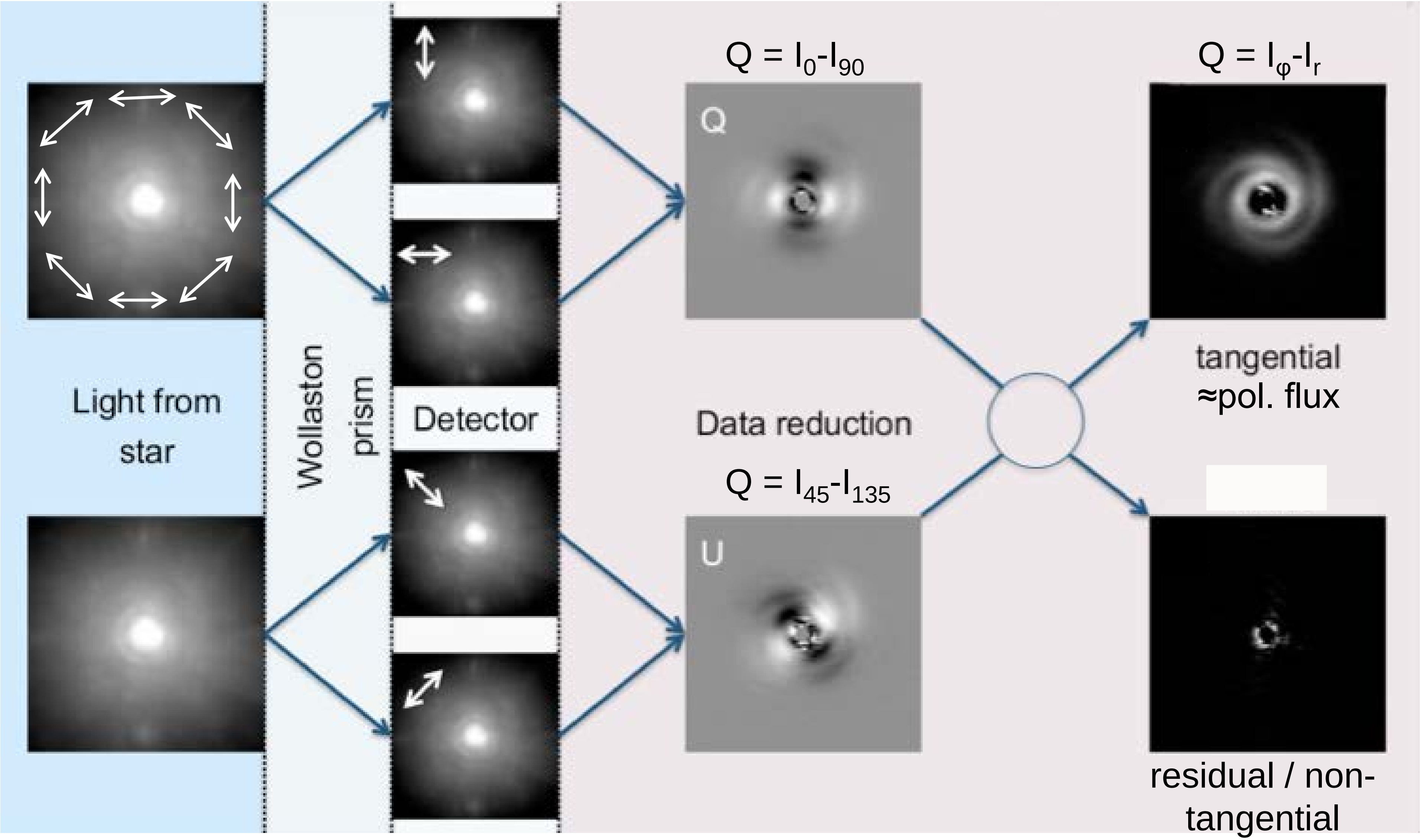

from H. Avenhaus

debris disks with DPI

(despite they are much fainter)

N. Engler et al.: HIP 79977 debris disk in polarized light

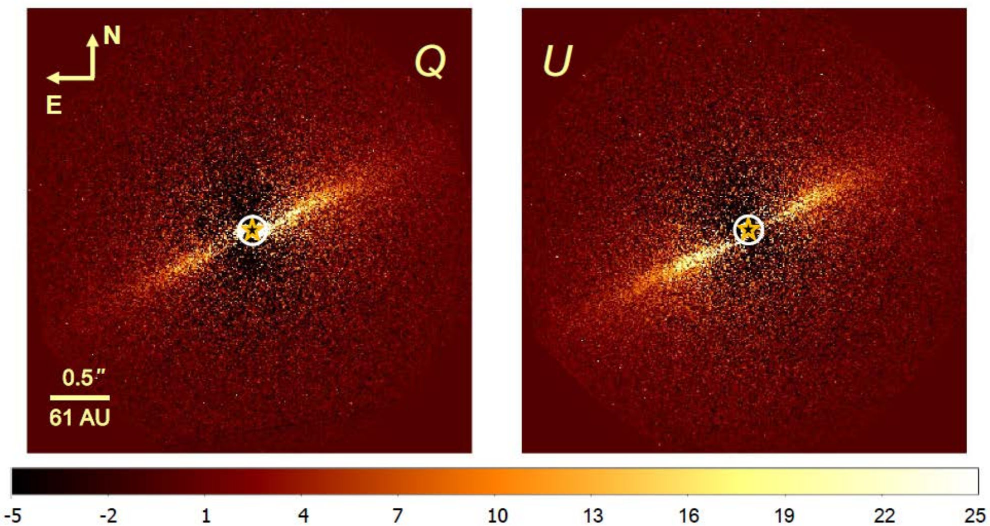

Fig. 3. Polarimetric differential imaging data of HIP 79977 with the VBB filter (590–880 nm). The mean images show polarized flux Stol (*left*) and *U* (*right*) after 3 × 3 binning. The position of the star is marked by an asterisk in orange. The image region located within a stellarcentric circle with a radius of ∼0.12″ is dominated by the strong speckles variations. The color-bar shows the counts per binned pixel.

optically thin dust scattering

→ radius of dust ring for edge-on disks

→ polarimetric scattering function

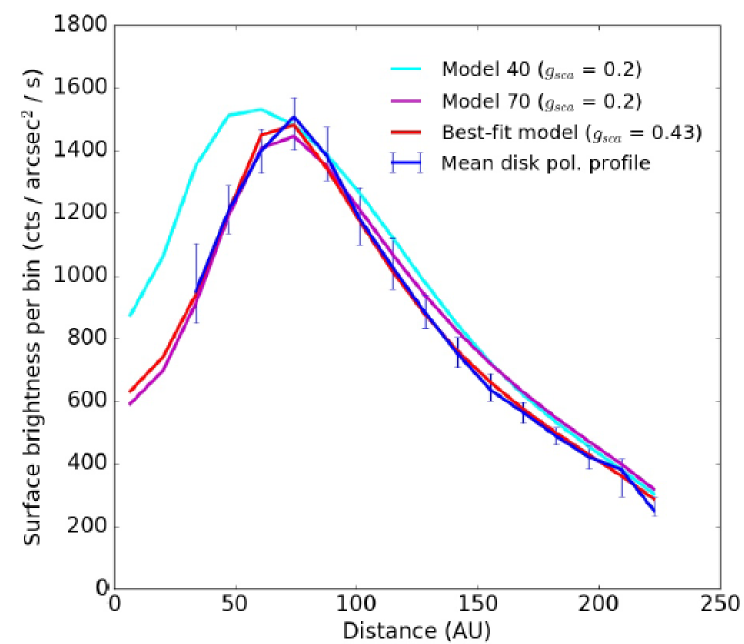

2. Observations of disks

Spectral energy distribution

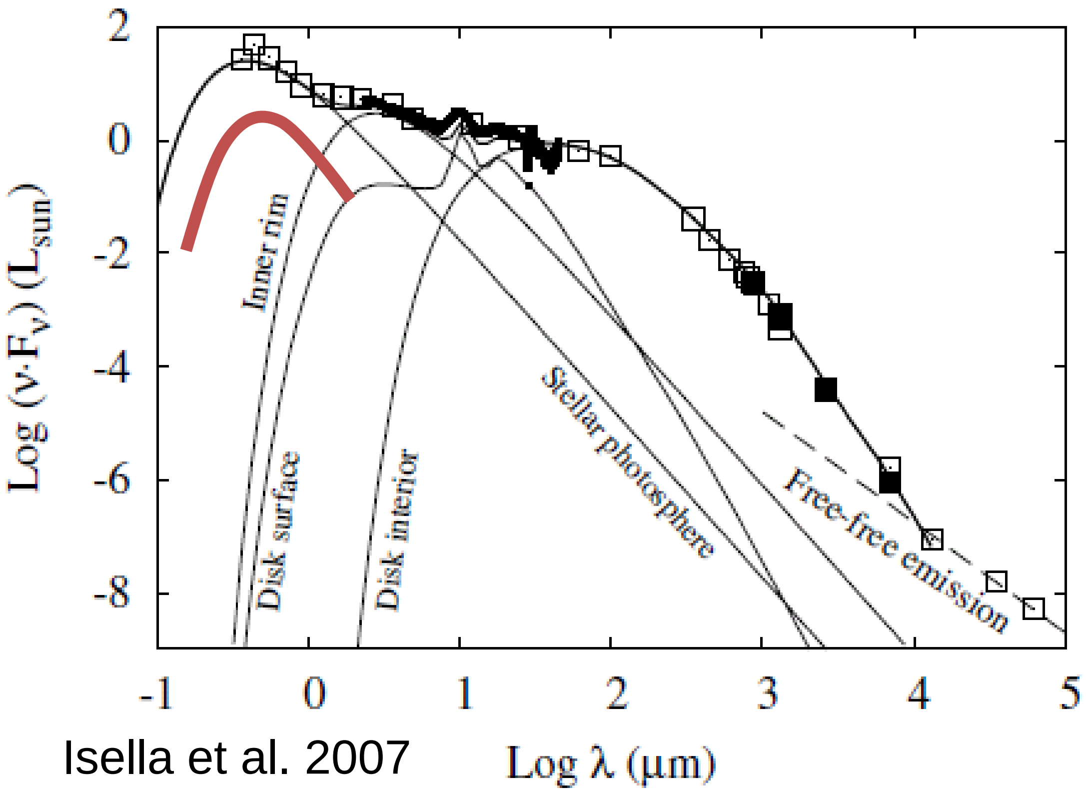

Isella et al. 2007

Scattered light (inner rim and disk surface)

Observations of disks

Spectral energy distribution

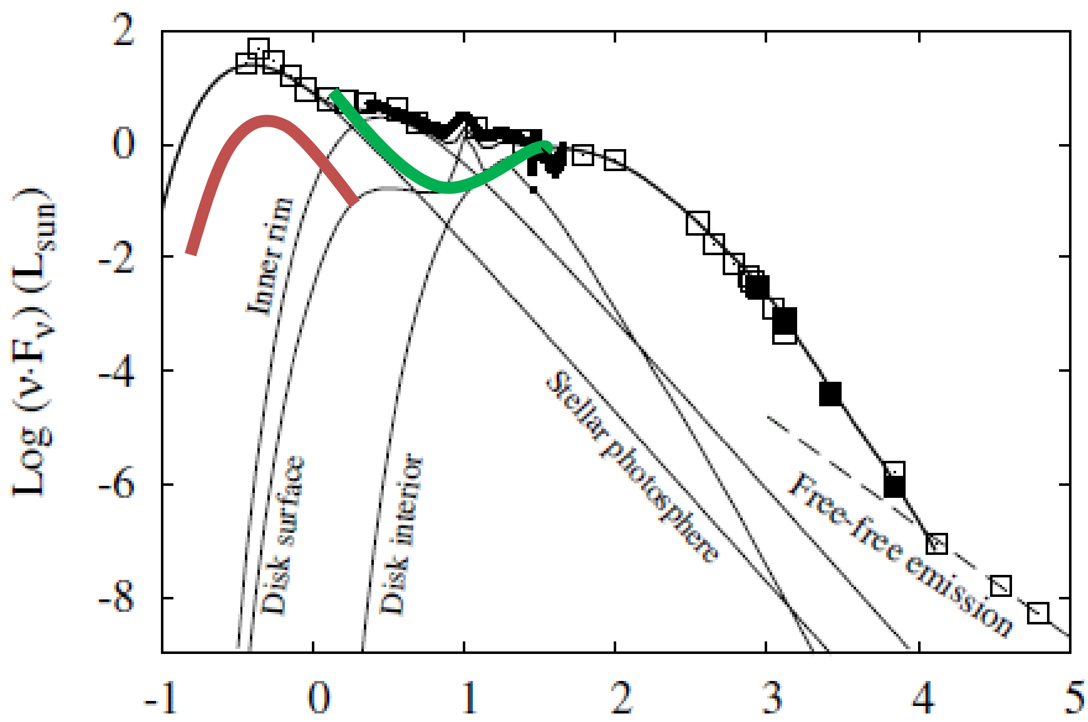

Isella et al. 2007

Mid-IR dip
→ inner gap in disk

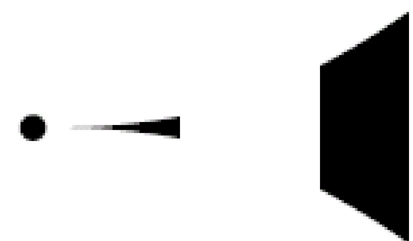

Transition disk (group I)

→ “normal”

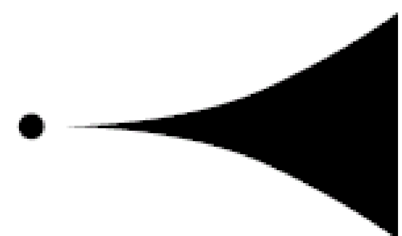

Primordial flaring disk

Statistics for protoplanetary disks

A. Garufi et al.: The evolution of protoplanetary disks, Group I vs. Group II

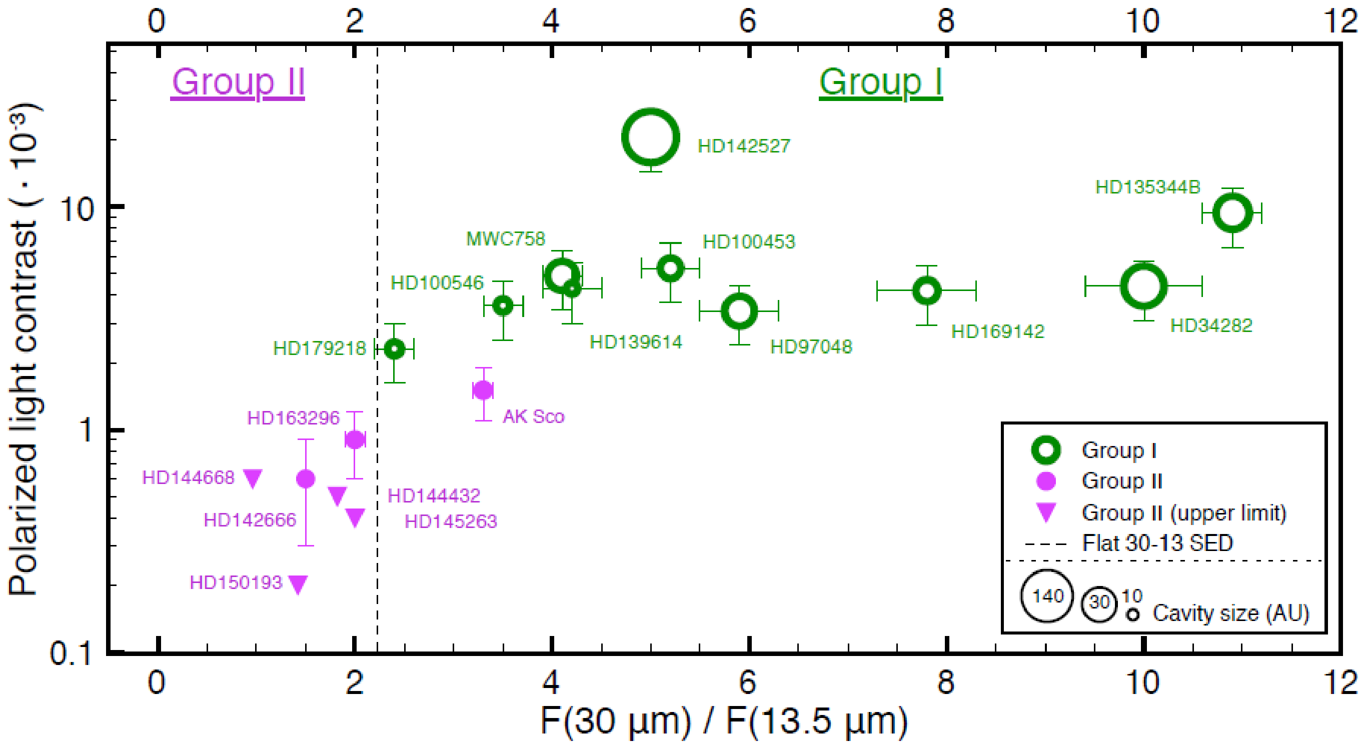

Fig. 3. Polarized-to-stellar light contrast for all the sources in the sample (see Appendix A) compared with the flux ratio at 30 μm and 13.5 μm. GI disks are plotted in green, GII in purple. The disk cavity, where known and as taken from different datasets (see text), is indicated by a gap in the symbol, proportional to the cavity size with dynamic range from 5 AU to 140 AU. The dashed line indicates the ratio corresponding to a flat SED, obtained from 30 ÷ 13.5 = 2.2. The ratios are from Acke et al. (2010), while the contrasts are from this work, as explained in Appendix B.

Different evolutionary phase or different evolutionary tracks?

A&A 603, A21 (2017)

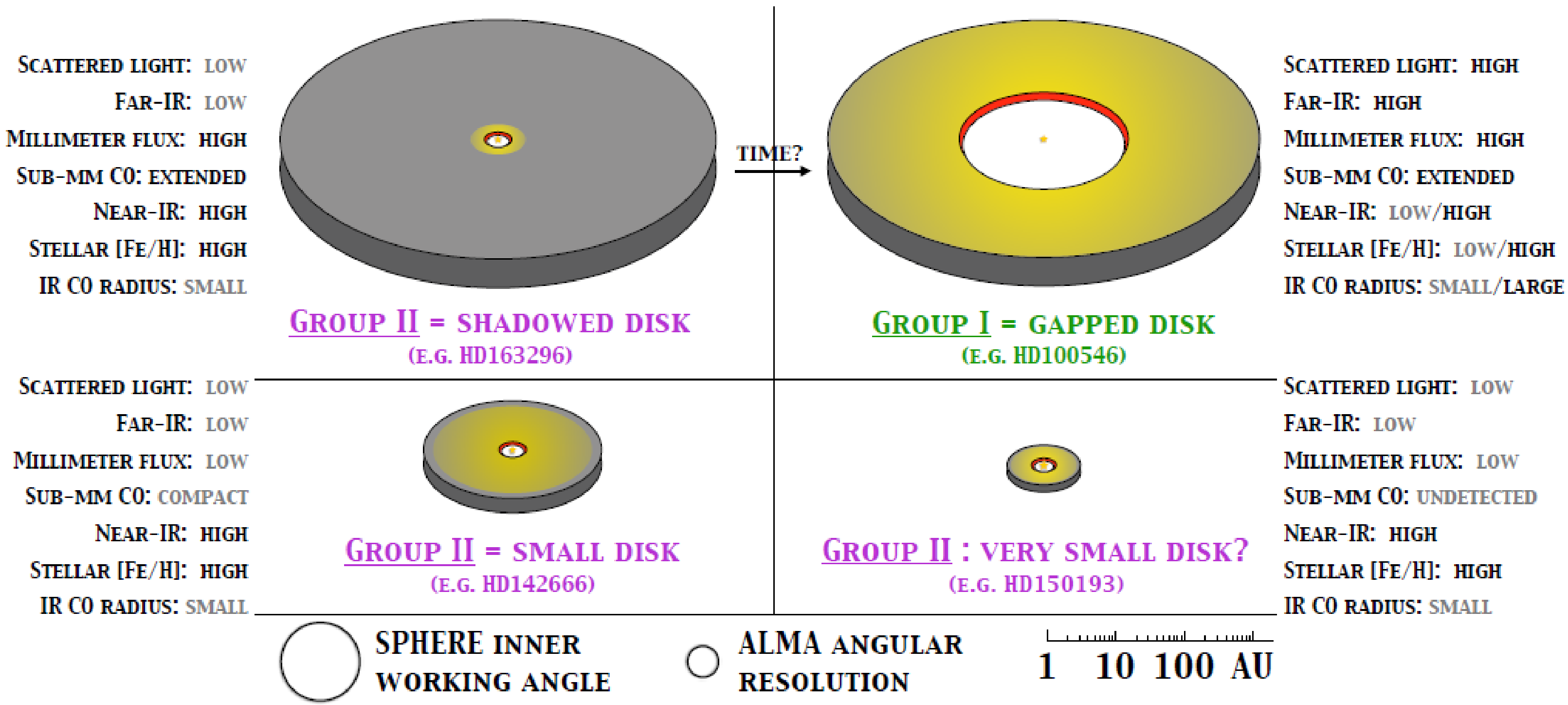

Fig. 7. Summary of the properties of the sources analyzed in this work. The proposed disk geometries are shown in logarithmic scale. The SPHERE inner working angle is imposed by the angular resolution of observations in the near-IR (~10 AU for sources at ~150 pc). The ALMA angular resolution of ~3 AU is achieved with the longest possible baselines, which should be used to resolve potentially very small disks.

see Garufi et al. 2017

ALMA thermal radiation and DPI scattered light

A specific case: SAO 206462

(Ph.D. thesis of Antonio Garufi)

2.2 µm
polarized light
VLT
(small particles)

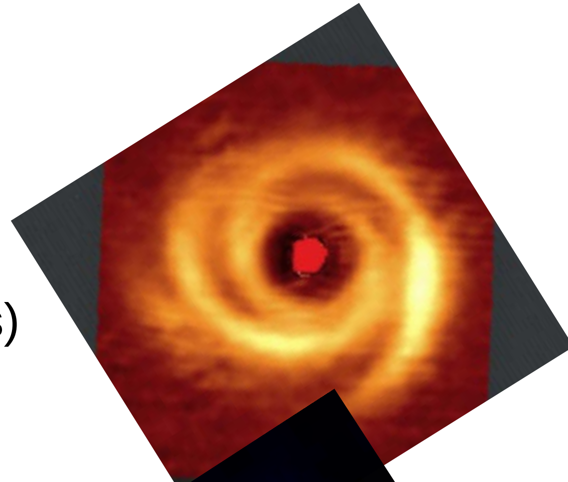

450 µm
ALMA
(large particles)

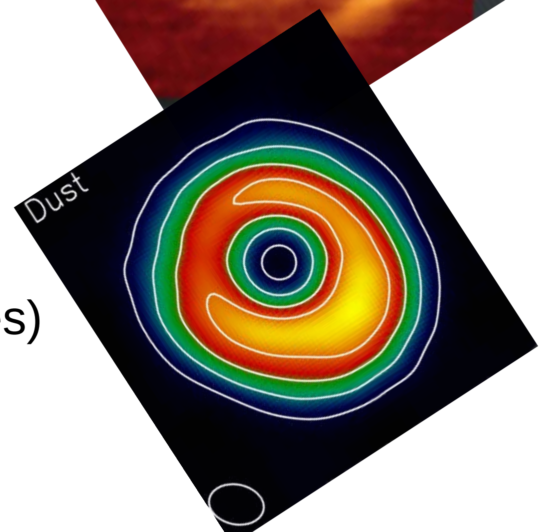

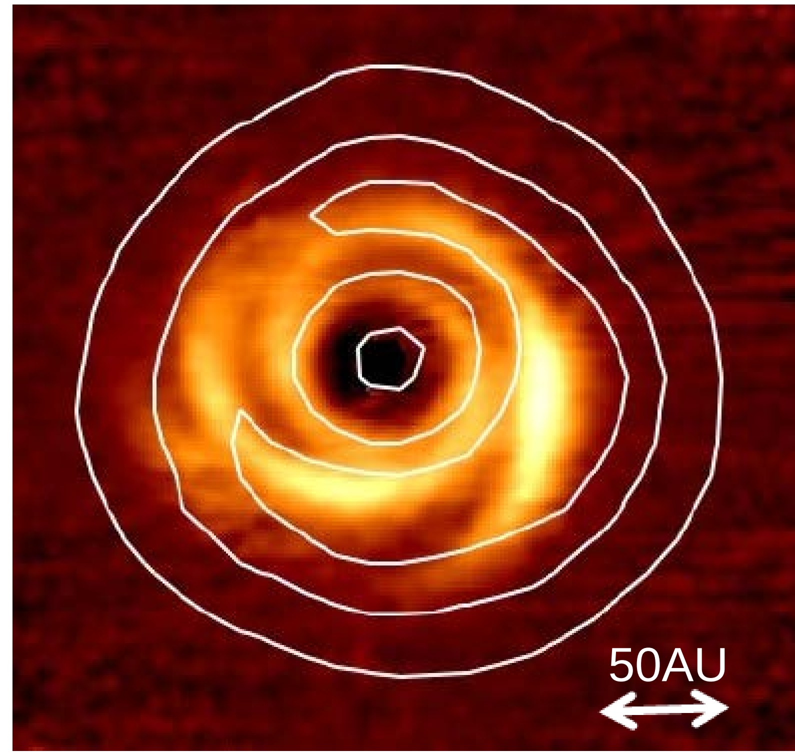

Inner cavity size: ≈ 30 AU for the scattering dust (small particles) and
≈ 40 AU for large particles according to the ALMA map

→dust size filtering by radial gas pressure "bump"

(predicted e.g. by Pinilla et al. 2012)

Accumulation of large grains in pressure bump induced by a planet in the gap

(from Garufi, Quanz et al. 2013)

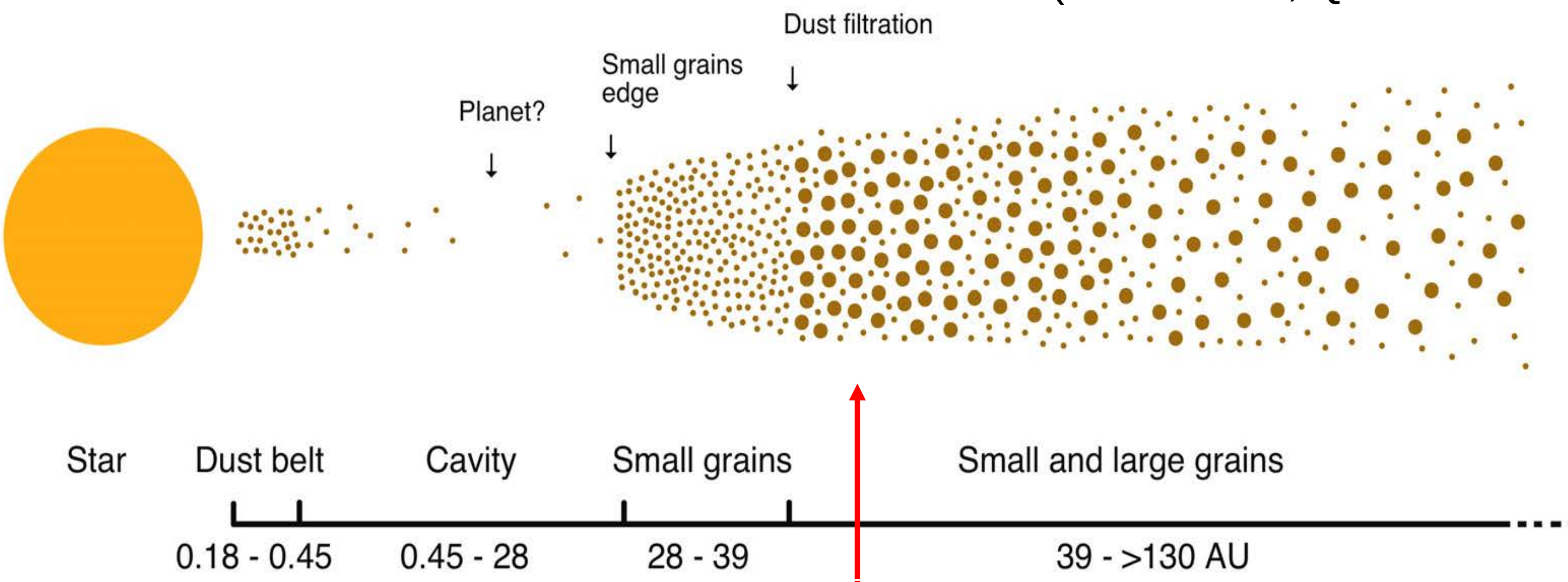

large grain accumulation region

gravity

dP/dr>0

gravity

dP/dr<0

motion of gas/small grains large grains "feel"

super-Keplerian backwind

sub-Keplerian headwind

Summary

SPHERE “VLT Planet Finder” → is the state of the art extreme AO system

the visual channel is quite special:

- high spatial resolution (20-30 mas)
- high contrast (ADI, SDI, PDI) and high dynamic range
- ZIMPOL fast-modulation polarimetry + pol. calibration

ZIMPOL opens many new research opportunites

- resolving the extended red giants
- Mapping of the light scattering from circumstellar dust (mass loss of evolved stars)
- Circumstellar Hα emission
- etc.

Search for reflecting planets around nearby stars

- Very deep limits are achieved – we keep trying a real detection!
- ZIMPOL is a good testbed for future instruments

Mapping of circumstellar disks

- SPHERE IRDIS and ZIMPOL DPI have huge impact on disk science
- Important complementary information to ALMA